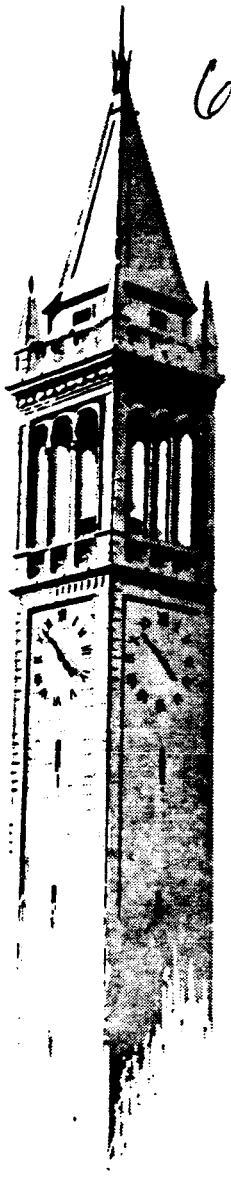

68p

EXPERIMENTAL INVESTIGATION OF THE EFFECTS OF TRANSPIRATION COOLING ON A PARTIALLY DISSOCIATED TURBULENT BOUNDARY LAYER

by

R. N. Meroney

Report No. AS-63-6
NASA Contract NAS8-850
November 15, 1963

INSTITUTE OF ENGINEERING RESEARCH
UNIVERSITY OF CALIFORNIA
Berkeley, California

CONTRACT NAS8-850
REPORT NO. AS-63-6
NOVEMBER 15, 1963

SPONSORED BY
NATIONAL AERONAUTICS AND
SPACE ADMINISTRATION

EXPERIMENTAL INVESTIGATION OF THE EFFECTS OF TRANSPIRATION COOLING ON A PARTIALLY DISSOCIATED TURBULENT BOUNDARY LAYER

by

R. N. Meroney

Submitted in partial satisfaction of
the requirements for the Masters Degree
in Mechanical Engineering

FACULTY INVESTIGATORS:

W. H. GIEDT, PROFESSOR OF AERONAUTICAL SCIENCES
C. L. TIEN, ASSOCIATE PROFESSOR OF MECHANICAL ENGINEERING

ABSTRACT

17576 A

The convective heat transfer between a partially dissociated combustion gas and a flat plate cooled by light gas injection (hydrogen or helium) was investigated experimentally. Gases were injected through a porous stainless steel test section instrumented with thermocouples to obtain local heat transfer rates. These heat transfer rates were computed from energy balances performed on the porous section undergoing steady state heating.

With injection of a light gas the local heat transfer rate decreased rapidly to an essentially uniform value within six inches of the leading edge. Variation of the blowing parameter $F = \rho_o v_o / \rho_e v_e$ from 0.005 to 0.01 decreased this uniform value of the heat transfer by 100%. Comparison of results with previous data showed agreement for helium. However, hydrogen injection resulted in heat fluxes up to 100% greater than those measured by other investigators. This suggests that the effectiveness of transpiration in reducing convective heat transfer will be reduced when dissociation of the injected series occurs.

Author

TABLE OF CONTENTS

LIST OF FIGURES

NOMENCLATURE

$C_f/2$	skin friction coefficient
C_H	Stanton number $q_w/\rho_e u_e C_{pe}(T_w-T_e)$
F	$\rho_w v_w/\rho_e u_e$ mass flow ratio
M	molecular weight of mixture
p	pressure
q_{cw}	convective heat transfer to wall
$q_c, q_{ms}, q_{rw_1}, q_{rw_2}, q_1, q_2$	defined in Section 3.1
R	universal gas constant
T	temperature
u	velocity parallel to plate
v	velocity perpendicular to plate
x	distance along plate from leading edge of injection region
y	distance normal to plate surface
z	thickness of porous section

Greek Symbols

α	thermal diffusivity
ϵ	emissivity of wall surface
λ	thermal conductivity
μ	absolute viscosity
ν	kinematic viscosity
$\xi = B$	blowing parameter $F/(C_f/2)$
ρ	density
σ	Stephan Boltzmann constant
τ	time interval

Subscripts

e	free stream value
H, H_2, CO	species designation
w	wall condition
∞	surrounds

All predictions tend to be extremely optimistic compared to experimental curves.[8] Also, most data available were obtained under low temperature potential conditions. Since the application of transpiration cooling will be made where high enthalpy conditions are encountered, further investigations of this area are definitely needed to increase confidence in the turbulent transpiration solutions and the empirical data to the level of that under laminar conditions.

During investigations made on the ablative properties of various phenolics it has become obvious that the part played by light gases generated in the carburizing surface upon the thermal boundary layer is very influential. The advantages of low molecular weight gas injection have been pointed out by several previous researchers.[6,9,10]

To facilitate the study of the injection of a light gas into a high temperature, turbulent, reactive boundary layer an existing oxy-acetylene flame apparatus mentioned in References 11, 12, and 13 was adopted. The flame apparatus provides a high temperature reactive heat source which simulates the problems of dissociated air at stagnation conditions on flight vehicles.[13]

The present report includes the description of an experimental study of transpiration cooling through a highly reactive turbulent boundary layer using two light gases, helium and hydrogen, as injected materials.

1.0 INTRODUCTION

The protection of a solid surface under conditions of intense thermal potentials has become important since the advent of rocket and satellite vehicles which travel at hypersonic speeds. Mass transfer in the form of transpiration, film cooling, or ablation has received particular attention as the best method available to reduce the extreme heat transfer rates encountered to acceptable magnitudes. In every case mass entering the boundary layer plays a dual role, for it (1) acts as a heat sink in, or on, the wall and (2) alters the heat transfer characteristics of the boundary layer as it leaves the wall. This is true regardless of whether the mass is introduced by mechanical transfer through porous walls or slots, or whether it enters in a self-controlling manner by sublimation or melting.

The transpiration of a light gas into a reactive turbulent boundary layer as a special subtopic of the larger problem deserves attention. Gas injection into laminar boundary layers has received the greater portion of all previous investigative efforts because it is amenable to more or less rigorous analytical solution. Extensive bibliographies covering this work may be found in References 1, 2, and 3. Turbulent boundary layers characteristically do not allow rigorous solution of the governing differential equations due to lack of knowledge concerning the turbulent exchange mechanisms. Most results are based on complex mixing length theories which require empirical data to accomplish a solution. Dorrance and Dore,[4] Rubesin,[5] and Van Driest[6] investigated analytically air injection into air, and Rubesin and Pappas[7] foreign gas injection into air, both under turbulent conditions. Unfortunately, Rubesin and Pappas' and Dorrance and Dore's results do not agree well with experimental results.

coils and degreased for acetylene service). This was done to reduce carbon formation during starting and stopping the flame. By turning the oxygen on first and the acetylene off first carbon formation and deposition are essentially eliminated. The impingement of carbon onto the porous plate was observed during preliminary runs. This problem also arose with previous investigators.[3]

2.2 Model Construction and Instrumentation

A 1/4 inch thick plate of porous stainless steel formed one wall of a plenum chamber. (See Figs. 4 and 5). The plate was instrumented with thermocouples which made possible the measurement of steady state heat fluxes. Due to the high temperatures and high heat rates involved, steps were taken to water cool the plenum chamber walls while minimizing conduction heat losses from the test specimen itself. The test section was constructed from a 3 × 6 inch by 1/4 inch thick piece of AISI 316 porous stainless steel. The mean pore opening was 0.0008 inches or 20 microns with a mean irregular particle diameter of 65 microns.* This size was chosen on the basis of recommendations of previous investigators.[14-18]

Figure 5 is a cross-section of the plate and chamber configuration. Side walls of the chamber were 0.008 inch thick AISI 304 stainless steel shim, which were copper and nickel-gold brazed to the porous plate and silver soldered to the oxygen-free copper bases.**

*Quoted by the manufacturer, Mirro Mettalic Corporation, a subsidiary of Pall Filtration Company.

**Leaks which arose during operation necessitated the addition of small retaining screws along the edges of the porous plate to stiffen the junction to the shim side walls.

2.0 EXPERIMENTAL EQUIPMENT AND PROCEDURE

The purpose of the experimental program was to obtain convective heat transfer rates to a flat plate under reactive turbulent flow conditions with as wide a range of transpiration and surface temperature conditions as possible. Hydrogen and helium were chosen for the injected gases because they are reputed to have the greatest effect on convective heat transfer per unit mass injected.[6,9,10] The convective heat transfer rate was equal to the sensible heat increase of the injected gas across a porous section plus the energy lost by radiation. Efforts were made to reduce conduction losses to a negligible amount.

Separate programs were carried out to determine free stream conditions at various distances from the leading edge and to specify the surface gas concentrations during injection.

2.1 Test System Arrangement

The test apparatus consisted of a multiple nozzle oxygen-acetylene flame head and a specimen holder and exhaust duct.[11] The equipment was so designed that when oxygen and acetylene were passed through the flame head and burned a two-dimensional high temperature gas stream was produced which provided parallel flow heating to a 3×6 inch test area. The average non-blowing heating rate has been measured to be approximately 40 BTU/ft^2sec.[13] The gas velocities were approximately 200 ft/sec with approximate gas temperatures of 5000 °F at atmospheric pressure. The general arrangement of the test area can be seen in Figs. 1, 2, and 3.

The manual starting valve for controlling the reacting gases was replaced by two normally closed solenoid valves (equipped with silver shading

The lower side of the plenum chamber was protected by cooling water coils. The seven upper chromel-alumel thermocouples were buttwelded and mounted in 0.016 × 0.016 inch slots in the surface of the plate; the seven lower thermocouples were spot welded along the bottom of the plate.[19] (See insert of Fig. 5). Care was taken to orient each thermocouple in an isothermal line normal to the flow direction. Small (0.032 inch o.d.) ceramic tubing electrically insulated the upper thermocouple lead wires from the plate. The tubes were held in place with high temperature Type A Astroceram cement which has a maximum service temperature of 4300 °F. Three 1/8 inch o.d. stainless steel surface concentration probe tubes were force-fitted into the porous plate, brought through the chamber, and sealed with fittings, as shown in the insert of Fig. 5. Bundles of thermocouple wires were potted into two short sections of copper tubing with epoxy resin and sealed in the plenum chamber wall with standard tube fittings. The transpirated gas entered the plenum chamber through a 1/8 inch diameter copper tube drilled to distribute the gas the length of the plenum chamber. The chamber was also instrumented to give plenum chamber gas temperature and pressure.

2.3 Velocity Measurements

To obtain approximate boundary layer momentum thicknesses and free stream velocity distributions, a water cooled stagnation tube and micrometer traversing mechanism were constructed. The experimental arrangement is shown in Fig. 3. The water cooled probe was designed with a 1/16 inch o.d. tube surrounded by a 1/4 inch o.d. copper water jacket. The water was not recirculating but exited upwards and back through three small jets on the top of the probe tip. During operation

these jets were observed to be deflected downstream and out the exhaust duct. The stagnation tube was attached to an inclined water manometer and had a time constant of approximately 5 seconds. Although measurements were restricted to distances greater than 0.030 inch from the plate, this was not considered disadvantageous since evaluation of measurements in a laminar sub-layer region with transpiration using an impact tube would be anomalous. The vertical traversing mechanism was a calibrated micrometer screw mounted under the specimen in such a manner that the probe could be moved to any desired position from the leading edge. A second screw provided a horizontal traverse.

Static pressure measurements indicated that atmospheric pressure conditions existed across the flame. Stagnation measurements were made at one inch intervals along the plate from the surface to midstream in 0.025 inch increments. Free stream velocities are plotted versus plate position in Fig. 6. A typical boundary layer velocity profile for blowing and nonblowing conditions depicts the turbulent character of the flow in Fig. 7.

2.4 Flame Temperature

The temperature in the gas stream was measured by the sodium line reversal technique. The general apparatus arrangement used has been described in Ref. 12; these measurements were made with an enclosed test section which reduced the free stream temperatures and velocities. The most satisfactory technique found for introducing sodium into the flame was to fasten short prisms of sodium hydroxide into an L-shaped jig attached to the micrometer screw located beneath the test section and to draw the salt down into the flame at a rate needed to maintain

a fairly constant flame brightness. It was also found that if a filter* was placed before the spectrometer entrance slit, the eye could perceive variations in background to line brightness with a greater accuracy.

Both the reference lamps and the optical pyrometer used were calibrated prior to the tests with an accurate standard. Most measurements were made along the length of the test section with no transpiration of hydrogen or helium into the boundary layer; however, one measurement was made near the end of the section with a very high injection rate at the surface ($F = 0.1$). No significant variation of free stream temperature due to transpiration could be found at this point.

Recent information available on the emissivity of TaC would predict that the brightness temperature of the reference light would closely approximate that of the flame as is assumed for tungsten lamps;[20,21] however, some of the measurements were repeated with tungsten lamps to check results. It is felt that, with the extra precautions taken, the final results for flame temperature shown in Fig. 6 are well within the ±150 °R range predicted by Russ.[12]

2.5 Radiation

The emissivity of the exhaust gas (considered to be "gray") was found by previous investigators to have a value of approximately 0.001.[12,22] An application of the Stefan-Boltzmann law shows that the radiation is a maximum of two percent of the smallest heating rate, which is insignificant.

Due to the porous nature of the surface a sintered material has been found to have an emissivity an order of magnitude larger

*Kodak Neutral Density No. 3 Wrattan Filter.

than that of conventional materials.[23] On this basis it was considered that radiation from the specimen surface would be significant. To determine the net radiative heat flux away from the plate two mirror-type directional radiometers (Leeds and Northrup Rayotubes) were positioned vertically over the apparatus. They viewed representative circles of about one inch in diameter on the surface. To separate the radiative flux of the gas from that of the plate, separate measurements were taken of the radiation from the flame alone.

2.6 Boundary Layer Composition

On the basis of a simple analysis by Denison[9] the boundary layer wall compositions may be calculated from the knowledge of the free stream concentrations and blowing parameter $B = \xi = (\rho_o v_o)/(\rho_e u_e)(2/c_f)$. However, since this is a critical step in the semi-analytical calculations of most existing heat transfer prediction schemes, it was considered important to make some experimental measurements.

Assuming the basic constituents of the equilibrium free stream are CO_2, H_2, CO, and H for a 1:1 fuel to oxygen ratio, with N_2 and O_2 possibly diffusing across the stream in small quantities, a gas analyzer of the micro-Orsat design was built.* (See Fig. 8.)

Gas samples were also analyzed by gas chromatography. Initially a modified Perkin and Elmer Vapor Fractometer Model 154 was used. This instrument had a low sensitivity for hydrogen and could not detect helium due to use of a helium carrier gas. Initial measurements verified, however,

*Unfortunately, the results of the operation of this apparatus were never felt to be valid due to the presence of leaks to the atmosphere. Hence all reported concentration results were determined by gas chromatography.

the assumption made in the calculation of transport properties for the helium injection case that the ratio of hydrogen to the carbon monoxide across the boundary layer remained essentially constant. Subsequent analyses were made on a Beckman GC-2 Gas Chromatograph using nitrogen as a carrier gas. Details of the chromatograph calibration and operation may be found in Appendix B.

Samples for analysis were obtained through stainless steel probes incorporated into the apparatus (see Fig. 5). Samples were taken during the test runs after steady state was reached, as indicated by the surface thermocouples. In order to insure a very weak suction which would not significantly affect the boundary layer an air-aspirator was used. Samples were removed from the probing system with a gas-tight hypodermic syringe and were stored in 8 cc evacuated medical serum bottles. The serum bottles remained gas tight over extended periods of time and were completely satisfactory as a transporting or storing medium. It was felt that drawing and storing samples at atmosphereic pressure would reduce the probability of contamination before analysis, as has been experienced by previous investigators.[24]

2.7 Transient Measurement of Zero Transpiration Heat Rates

To establish a basis for the comparison of results the zero-transpiration heat rates to the wall surface need to be known. An AISI 304 stainless steel calorimeter plate (1/8" × 3" × 6") was instrumented with six chromel-alumel thermocouples in the manner described by Russ[12] and Cobb[25]. This plate was mounted flush with the GR 28 firebricks and positioned 1/4 inch below the bottom row of flame nozzles, and two inches downstream from the nozzles. Thermocouple outputs were recorded on a Honeywell Visicorder.

2.8 Test Procedure

The porous plate was cleaned carefully to remove oils from handling and construction. The plate was then positioned parallel to the oxyacetylene flame path 1/4 inch below the bottom row of nozzles and with its leading edge two inches downstream from the nozzles. The plate was surrounded with carefully cut and fitted GR28 firebricks to present a continuous flat surface to the flame.* Continuous tracings of the 16 thermocouples' output were obtained with a Minneapolis Honeywell 906A-L Visicorder. Since there were only nine of the direct current operated galvanometers available for the Visicorder, the thermocouples were circuited through a set of relays, and a commutating device alternated the signals to the Visicorder.

The recorder galvanometers were calibrated before and after each series of test runs for each temperature range to insure accuracy. No significant deviations occurred.

Hydrogen or helium was drawn from two pressure bottles manifolded together outside the building and regulated by two gas regulators. Flow rates were measured with Fischer and Porter Flowrators. The temperatures and pressures of the gases were measured at the flowrators to permit accurate calculation of mass flow rates.

During the starting period of each run argon or helium rather than hydrogen was transpirated through the plate. Before extinguishing the flame, argon was again introduced into the plenum chamber and the hydrogen flow turned off by means of a three-way valve. Such a precaution prevented ignition of the hydrogen and purged lines leading to the plenum chamber. (This precaution was not necessary for helium operation.)

*During a number of the test runs the bricks were replaced by a fitted water cooled brass plate.

3.0 HEAT TRANSFER AND VELOCITY DISTRIBUTIONS

3.1 Convective Heat Transfer Distribution

The test records provided a set of steady state temperature readings, injected gas mass flow rates, and total radiation radiometer readings. The convective heat flux to the plate is calculated from the following energy balance: (See Fig. 9).

$$q_c = q_{ms} + q_{rw_1} + q_{rw_2} + q_{1b} - q_{1a} - q_{rg} \tag{3.1}$$

where q_c is the heat transferred from the boundary layer by conductive and diffusive mechanisms in the gas; q_{rw_1} and q_{rw_2} are heat rates of radiation away from the plate; q_{ms} represents the increase in sensible heat of the injected gas; q_{1a} and q_{1b} are heat rates of energy conducted in and out of the element in the direction along the plate; and q_{rg} is the heat rate of radiation from the gas to the plate surface.

Since the tests were run with the plate unenclosed, the net radiation between a differential surface area of the plate and the black room surrounds is:

$$q_{rw_i} = \epsilon_p \sigma (T_{w_i}^4 - T_\infty^4) \tag{3.2}$$

The total emissivity may be determined from radiometer readings. The radiometer measures the total energy radiated by the test surface (E_w) plus the radiation of the flame in the normal direction (E_ϵ). Assuming that the emissivity is independent of direction, the Stefan-Boltzmann law can be written as:

$$E_g + E_w = \sigma T_{bR}^4 \tag{3.3}$$

when the radiometer looks through the flame at the surface. Similarly, when the radiometer looks at the flame only:

$$E_g = \sigma T_{bR_f}^4 \tag{3.4}$$

hence:

$$\epsilon_p = \frac{T_{bR}^4 - T_{bR_f}^4}{T_w^4} \tag{e.5}$$

Therefore the total emissivity of the specimen surface at any given temperature can be found from the radiometer and thermocouple readings.*

The rate of increase of the sensible energy of the injected gas is given by:[26]

$$q_{ms} = (\rho v)_c \left[h(T_w) - h(T_c)\right]_{H_2} \tag{3.6}$$

The temperature of the coolant leaving the plate surface will be that of the plate surface.[17,27]

The net rate of conduction through the elemental volume is given by the relation:

$$q_{1a} - q_{1b} = k_m z \left(\frac{d^2T}{dx^2}\right)_m \tag{3.7}$$

where k_m is the thermal conductivity of the specimen, and $(d^2T/dx^2)_m$ is the second derivative of the mean temperature distribution of the upper and lower porous plate surface temperatures.

*Evaluation of the radiometer output for each run reveals an average total emissivity of 0.65. This value is of the order of magnitude predicted by Eckert for such a porous material.[23]

Therefore, at any one location on the plate surface, the convective heat rate per unit surface area may be found from:

$$q_c = (\rho v)_c \left[h(T_w) - h(T_c)\right]_{H_2} + \epsilon_p \sigma \left(T_{w_1}^4 + T_{w_2}^4 - T_\infty^4\right) - k_m z \left(\frac{d^2T}{dx^2}\right)_m - \epsilon_g \sigma T_g^4 \qquad (3.8)$$

Studies of gas flow through a plane wall of a porous material have revealed the following relationship between mass flow rate and the several governing parameters[28]

$$\frac{(\rho v)_c}{\mu} \sim \left(\frac{P_1^2 - P_2^2}{\mu^2 T_z}\right)^{1/2} \qquad (3.9)$$

Since the pressure difference across the porous section may be assumed constant, variations in local mass flow rate depend on the local wall temperature and its effects on viscosity. Hence one may write for the local injection mass rate

$$(\rho v)_c = (\rho v)_{cL} \left(\frac{T_L}{T_w}\right)^{1/2} \qquad (3.10)$$

where it has been assumed viscosity varies inversely with temperature, and $(\rho v)_L$ is

$$(\rho v)_{cL} = \frac{G}{w \int_0^L \left(\frac{T_L}{T_w}\right)^{1/2} dx}$$

where G = total mass flow of coolant lb_m/sec

w = width of porous section

T_L = wall temperature at position 6 inches downstream from leading edge of porous section

T_w = local wall temperature.

The thermal conductivity of porous stainless steel AISI 316 may be obtained from the following relation:

$$k_m = \rho\, c_m\, \alpha_m$$

where ρ = density of porous stainless steel

c_m = thermal capacity of AISI 316 stainless steel[29]

α_m = experimental thermal diffusivity of porous stainless steel.

The variation of α with temperature was measured experimentally by a transient technique outlined in Appendix A as developed by Boozer.[30]

3.2 Velocity Profiles

Because of the low velocities there were no compressible characteristics such as shock waves to complicate the evaluation of the stagnation pressures measured by the pitot tube; hence the velocity was related to the stagnation pressure by:

$$u = \left[2g \frac{P_o - P}{\rho} \right]^{1/2}$$

The density in the stream, however, varied widely because of the large temperature changes. Assuming that large light gas concentrations were confined to the laminar sublayer, the following assumption based on Reynolds' analogy for Pr close to 1 was used:

$$\frac{T - T_w}{T_e - T_w} = \frac{u}{u_e}$$

and from the perfect gas law:

$$\rho = \frac{pM}{RT}$$

By choosing $M = 19.34$ this closely matches actual density conditions over a wide temperature range.[31]

Substituting the latter two relations into the first gives finally:

$$u = \left[\frac{g\ R\ (T_e - T_w)(p_o - p)}{M\ u_e\ p} \right] + \left[\left(\frac{g\ R\ (T_e - T_w)(p_o - p)}{M\ u_e\ p} \right)^2 + 2 \left(\frac{R\ (p_o - p)\ g\ T_w}{M\ p} \right) \right]^{1/2} \qquad (3.11)$$

where $(p_o - p)$ is determined from the water manometer reading by:

$$(p_o - p) = \frac{\gamma\ \Delta\ h}{12}$$

Although the above expression is not precise, we may assume fair accuracy for turbulent boundary layers and $Pr_T \approx 1$. The velocity profiles were used to calculate momentum thicknesses for the boundary layer which eventually led to the determination of an equivalent leading edge position. The characteristic shape of the velocity profile also verified that the boundary layer had not separated from the plate due to transpiration velocities. (See Fig. 7).

3.3 Evaluation of Calorimeter Plate Results

Test results yielded a temperature history of the centers of several one inch sections of the plate. The heat flux is calculated from

the calorimeter equation:

$$q_p = \rho z c \frac{dT}{d\tau} \tag{3.12}$$

where ρ = plate density

z = plate thickness

c = heat capacity of plate material

$dT/d\tau$ = slope of temperature history.

A portion of the thermal energy passes through the calorimeter plate into the support brick. If one assumes the brick is a semi-infinite solid subjected to a linear temperature rise, then one may write:

$$q_b = \lambda \frac{2 A \tau}{\sqrt{\pi \alpha \tau}} \tag{3.13}$$

where λ = thermal conductivity of brick

A = slope of surface temperature history

τ = time

α = thermal diffusivity of brick

Total heat flux is the sum of (3.12), (3.13), and a radiation term, hence:

$$q_w^\circ = z c \frac{dT}{d\tau} + \lambda \frac{2 A \tau}{\sqrt{\pi \alpha \tau}} + \epsilon_p \sigma T_w^4 \tag{3.14}$$

4.0 DISCUSSION OF RESULTS

4.1 Heat Rate Distributions

Data were taken at four different transpiration conditions throughout the available range. The upper limit was determined by the maximum injection rate the boundary layer would withstand without separation, and the lower limit was determined by the maximum temperatures at which the brazed joints of the porous plenum chamber could be expected to remain intact. The consistency of experimental data from run to run under the same transpiration condition was very satisfactory. The flame side (upper) and the coolant gas side (lower) steady state temperatures of the porous plate are plotted versus position in Figs. 10, 11, 12, and 13, for the different injection rates. The effect of end losses to the forward plenum chamber wall is evident.

Only the maximum transpiration rate of helium was studied because the steady state temperatures of the equipment were in the critical range. The local heat transfer rates to the wall were calculated by the procedure described in Section 3.1. The ratio of these quantities to the no-transpiration heat rates obtained by a calorimeter plate (See Sections 2.7 and 3.3), is plotted in Fig. 14 versus plate position. The average value of the blowing parameter F was 0.01; however, due to the wall temperature variation, the actual local injection rates varied from 0.0088 at the leading edge to 0.0130 at the trailing edge. The injection of helium ($F \simeq 0.01$) reduced the heat transfer ratio q/q_o from 1 at the leading edge to 0.24 at the trailing edge. This reduction appears to be asymptotic in nature, and it may be supposed that extrapolation of injection effects to points further downstream would show comparatively small further reductions.

Three transpiration conditions were studied with hydrogen injection. The average values of the blowing parameter were 0.01, 0.0066, and 0.005. The actual injection ranges varied from 0.0066 to 0.0115, 0.0045 to 0.0081, and 0.004 to 0.0063, respectively. The ratios of the local heat transfer rates to the local zero transpiration values are plotted in Fig. 15 versus plate position. The injection of hydrogen ($F \simeq 0.1$) reduced the heat transfer ratio q/q_o to 0.18 in six inches. Hydrogen injection at $F \simeq 0.005$ reduced the heat transfer ratio to 0.37 in the same plate length. Hence a 100% increase in blowing rate (from 0.005 to 0.01) reduced the heat transfer ratio at the trailing edge by 100% also.

4.2 Surface Concentration Measurements

Results of the analysis of gas samples from the one, two, and three inch positions along the plate for the various runs are plotted in Figs. 16 and 17. All data shown were obtained with a Beckman GC-2 Gas Chromatograph using a nitrogen carrier gas. The evaluation technique is outlined in Appendix B.

The wall mass fractions for hydrogen injection, for which more data points are available, are internally consistent; that is, the higher injection rates produce higher wall mass fractions. The helium data display the expected lower values in the initial injection region which increase in the downstream direction. The need for more data is apparent. More samples were taken than the data points presented. Unfortunately, results were not obtained from the others due to erratic chromatograph behavior. The placement of the sample probes was made with the intention of rotating the test section 180° to obtain further concentration data at downstream positions. This idea was not pursued because of erratic torch and chromatograph behavior.

The dashed lines on Figs. 16 and 17 represent wall mass fractions based on calculations using the methods of Rubesin and Pappas[6] or Ness.[10] The experimental data in the leading edge region is lower than that predicted. A program including more samples at more locations is necessary before final conclusions can be drawn.

4.3 Error Analysis

To determine the validity of the experimental results reported herein an error analysis was made to find the probable propagation of randon errors into the final results as displayed on the various figures. The evaluation technique is incorporated in Appendix C. Wall temperature measurements shown in Figs. 10 to 13 were found to include a probable accuracy of 5%. The non-transpiration heat fluxes calculated would normally vary no more than 4.25%. The resulting accumulated probable error in the heat transfer ratio q/q_o is 6.7% for helium injection and 7.7% for hydrogen injection. The results included in Fig. 18 have their ranges of probable error indicated by limiting crosses.

Consideration of the data in Figs. 10 through 13 will indicate variations which obviously exceed those suggested by the error analysis. It is evident that systematic errors are present despite care taken to minimize their appearance. Smoothing curves were drawn commensurate with the author's experience with the equipment operation.

4.4 Comparison with Previous Investigations

Comparison of the data obtained in this investigation for helium and hydrogen gas injection with previous results is made in Fig. 18, where q/q_o is plotted versus $C_{p_i} F(x)/C_{p_e} C_{Ho}(x)$. Use of the latter parameter

has been proposed by Woodruff;[8] it is similar to the quantity previously suggested by Eckert.[32] As can be noted, the helium injection data fall among previous data near the average curve determined by Woodruff; however, the hydrogen data points are above the curve as much as 100%.

The most obvious difference between the conditions experienced with the hydrogen injection studied herein and that of previous investigators is that the transpirated gas experiences temperatures which are capable of dissociating it into atoms. If such a condition can result in lower effective blockage of heat to the wall than has been previously experienced at lower temperatures, the internal mechanisms of microscopic and macroscopic flow deserve further study. Recent design analyses have suggested the protection of missile skins under hypersonic flight conditions using hydrogen as a transpirated gas--present results suggest caution in such an application.

Comparison of Figs. 14 and 15 reveals that the reduction in heat transfer ratio in the leading edge region was greater for helium than for hydrogen at equivalent blowing rates. Although this behavior may be associated with the results discussed above, an alternative suggestion might be that the hydrogen was combining with air entrapped in the burning acetylene mixture at the torch tips. Barber[33] investigated hydrogen injection in a stagnation region and measured heat transfer ratios q/q_o greater than unity. He concluded that this result was due to hydrogen combustion in the boundary layer.

5.0 RECOMMENDATIONS

The evidence of this experimental study indicates further research should be centered around the following points:

1. The ideas suggested by hydrogen injection and dissociation at high temperatures should be examined. It must be determined if the rise in heat transfer ratio observed with hydrogen is in truth due to dissociation and its effect on concentration gradients.
2. The techniques used to determine experimental wall concentrations used herein do not appear adequate. Since the wall mass fractions will be an important boundary condition in any analysis, an accurate measurement of these quantities is necessary to verify any theory proposed.

Further experimental investigation of the transpiration cooling problem using the equipment outlined in this report would not appear to be advisable until analysis reveals more about the internal nature of the heat transfer mechanism under dissociation conditions.

6.0 CONCLUSIONS

On the basis of the results obtained in this experiment the following conclusions may be drawn:

1. Injection of low molecular weight gases such as helium and hydrogen may reduce by 80% total heat transfer rates through surfaces encountering turbulent boundary layer flows.

2. An increase by a factor of 100% in such injection rates may reduce the heat transfer rates by a factor of 100% also.

3. The application of hydrogen as a transpiration agent in conditions where dissociation may occur should be approached with caution due to the failure of hydrogen in this experiment to reduce heat transfer to the extent previously observed under non-dissociation conditions.

4. In view of the importance of the wall mixture concentration, and in view of the disagreement between measured wall mass fraction conditions and those predicted by present analytical mathods, attention should be directed both toward further analytical effort and better measuring techniques.

REFERENCES

1. J. F. Gross, J. P. Hartnett, D. J. Masson, & C. Gazley, Jr., "A Review of Binary Boundary Layer Characteristics," RAND Corp., Santa Monica, Calif., Report P1729 (1959).

2. H. S. Mickley, R. C. Ross, A. C. Squyers, & W. E. Stewart, "Heat Mass and Momentum Transfer for Flow Over a Flat Plate with Blowing or Suction," NACA TN-3208 (1959).

3. C. C. Lin, ed., Turbulent Flows and Heat Transfer, (Vol. II, High Speed Aerodynamics and Jet Propulsion Series), Princeton Univ. Press, Princeton, N. J. (1959).

4. W. H. Dorrance & F. J. Dore, "The Effect of Mass Transfer on the Compressible Turbulent Boundary Layer Skin Friction and Heat Transfer," J. Aero. Sci. 21, 404 (1954).

5. M. W. Rubesin, "An Analytical Estimation of the Effect of Transpiration Cooling on the Heat Transfer and Skin Friction Characteristics of a Compressible, Turbulent Boundary Layer," NACA TN-3341 (1954).

6. E. R. VanDriest, "On the Mass Transfer Near the Stagnation Point," RAND Symposium on Mass Transfer Cooling for Hypersonic Flight, June (1957).

7. M. W. Rubesin & C. C. Pappas, "An Analysis of the Turbulent Boundary Layer Characteristics on a Flat Plate with Distributed Light-Gas Injection," NACA TN-4149 (1958).

8. L. W. Woodruff, (Unpublished Report), Boeing Aircraft Company, D2-22202, Seattle, Wash. (1962).

9. M. R. Denison, "The Turbulent Boundary Layer on Chemically Active Ablating Surfaces," J. Aero. Sci. 28, 271 (1961).

10. N. Ness, "Foreign Gas Injection into a Compressible Turbulent Boundary Layer on a Flat Plate," J. Aero. Sci. 28, 645 (1961).

11. D. Wizansky & E. J. Russ, "An Oxyacetylene Flame Apparatus for Surface Ablation Studies," Univ. of Calif. Eng. Proj. Report HE-150-167 (1959).

12. E. J. Russ, "Heating Rate Characteristics of an Oxyacetylene Flame Apparatus for Surface Ablation Studies," Univ. of Calif. Eng. Proj. Report HE-150-176 (1959).

13. W. H. Giedt, "Investigation of the Behavior of Reinforced Plastics Subjected to Low Heating Rates," Final Report, Contract DA-04-200-ORD-776 (1961).

14. P. Duwez and J. Wheeler, "Experimental Study of Cooling by Injection of a Fluid Through a Porous Material," J. Aero Sci. 15, 9 (1948).

15. L. Green, Jr., & P. Duwez, "Fluid Flow Through Porous Metals," J. Appl. Mech., ASME Trans. 72, 39 (1951).

16. N. P. W. Moore & P. Grootenhuis, "Some Observations on the Mechanism of Sweat Cooling," Proc. Int'l Congress for Applied Mechanics 3, 106, London (1948).

17. P. Grootenhuis, "Flow of Gases Through Porous Metal Compacts," Engineering 167, 291 (1949).

18. P. Grootenhuis, "The Mechanism and Application of Effusion Cooling," J. Royal Aero. Soc. 63, 578 (1959).

19. W. E. Brunk, "Experimental Investigation of Transpiration Cooling for a Turbulent Boundary Layer in Subsonic Flow Using Air as a Coolant," NACA TN-4091 (1957).

20. S. S. Penner, Quantitative Molecular Spectroscopy and Gas Emissivities, Addison-Wesley Pub. Co., Inc., London (1959).

21. J. A. Coffman, "Carbonization of Plastics and Refractory Materials Research Program," General Electric Co. Quarterly Report #2, (1960). (ASTIA AD-236-160).

22. L. W. Woodruff, "Heat Transfer from Partially Dissociated Combustion Gases to a High Temperature Surface," Univ. of Calif. Eng. Proj. Report HE-150-199 (1962).

23. E. R. G. Eckert, J. P. Hartnett, & T. F. Irvine, Jr., "Measurement of Total Emissivity of Porous Materials in Use for Transpiration Cooling," Jet Propulsion 26, 280 (1956).

24. R. Y. Mixer, P. L. Chamberlain, & C. W. Marynowski, " A Study of the Mechanism of Ablation of Reinforced Plastics," Stanford Research Institute, Quarterly Report No. 4 (1959), p. 9.

25. L. L. Cobb, Jr., "The Influence of Hydrogen Recombination on Turbulent Flow Heat Transfer to a Flat Plate," Univ. of Calif. Eng. Proj. Report HE-150-183 (1960).

26. J. Hilsenrath, et.al., Tables of Thermodynamics and Transport Properties, Pergamon Press, London (1960). (NBS Circular 564).

27. O. E. Tewfik, E. R. G. Eckert, & L. S. Jurewicz, "Measurement of Heat Transfer from a Circular Cylinder to an Axial Stream with Air Injection into Turbulent Boundary Layer," Heat Transfer Lab., Univ. of Minn., Tech. Note No. 38 (1961).

28. P. L. Donoughe & R. A. McKinnon, "Experimental Investigation of Air Flow Uniformity and Pressure Level on Wire Cloth for Transpiration-Cooling Applications," NACA TN-3652 (1956).

29. Physical Constants of Some Commercial Steels at Elevated Temperatures, "Table IIIC, Specific Heats of High Alloy Steels," Butterworths Scientific Publications, London (1953).

30. G. D. Boozer, " A Method of Measuring the Thermal Diffusivity of Consolidated Materials at Elevated Temperatures," M. S. Thesis, Univ. of Calif., (1958).

31. S. R. Brinkley, H. E. Edwards, & R. W. Smith, "The Thermodynamics of Combustion Gases," Bureau of Mines Report 4958 (1953).

32. E. R. G. Eckert, "Survey of Boundary Layer Heat Transfer at High Velocities and High Temperatures," Wright Air Development Center Tech. Report 59-624 (1960) (ASTIA AD-238-292).

33. E. A. Barber, "An Experimental Investigation of Stagnation Point Injection," Boeing Co., Seattle, Wash. Report 63-433 (1963). (Presented at AIAA Conference on Physics of Entry into Planetary Atmospheres, M.I.T. (1963).

34. F. Agha, "Gas Chromatography Application to Exhaust Gas Analysis," Thesis, Mech. Eng., Univ. of Calif. (1962).

35. T. Johns, "Gas Chromatography Applications Manual," Bulletin 756-A, Beckman Instruments, Inc. (1960).

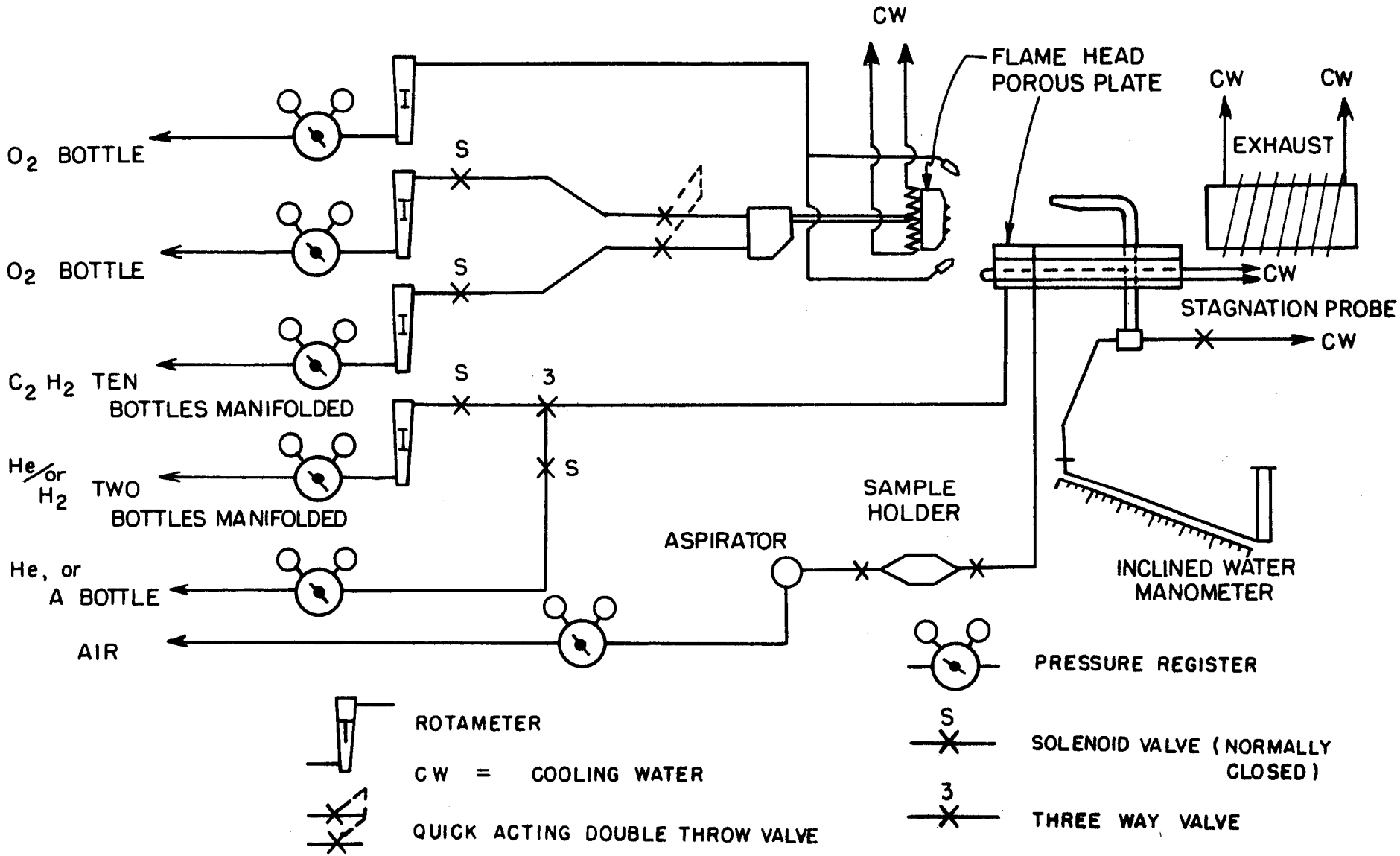

FIG. 1 OXY-ACETYLENE FLAME HEAD, POROUS PLATE, AND SUPPORTING EQUIPMENT

HYD 8049

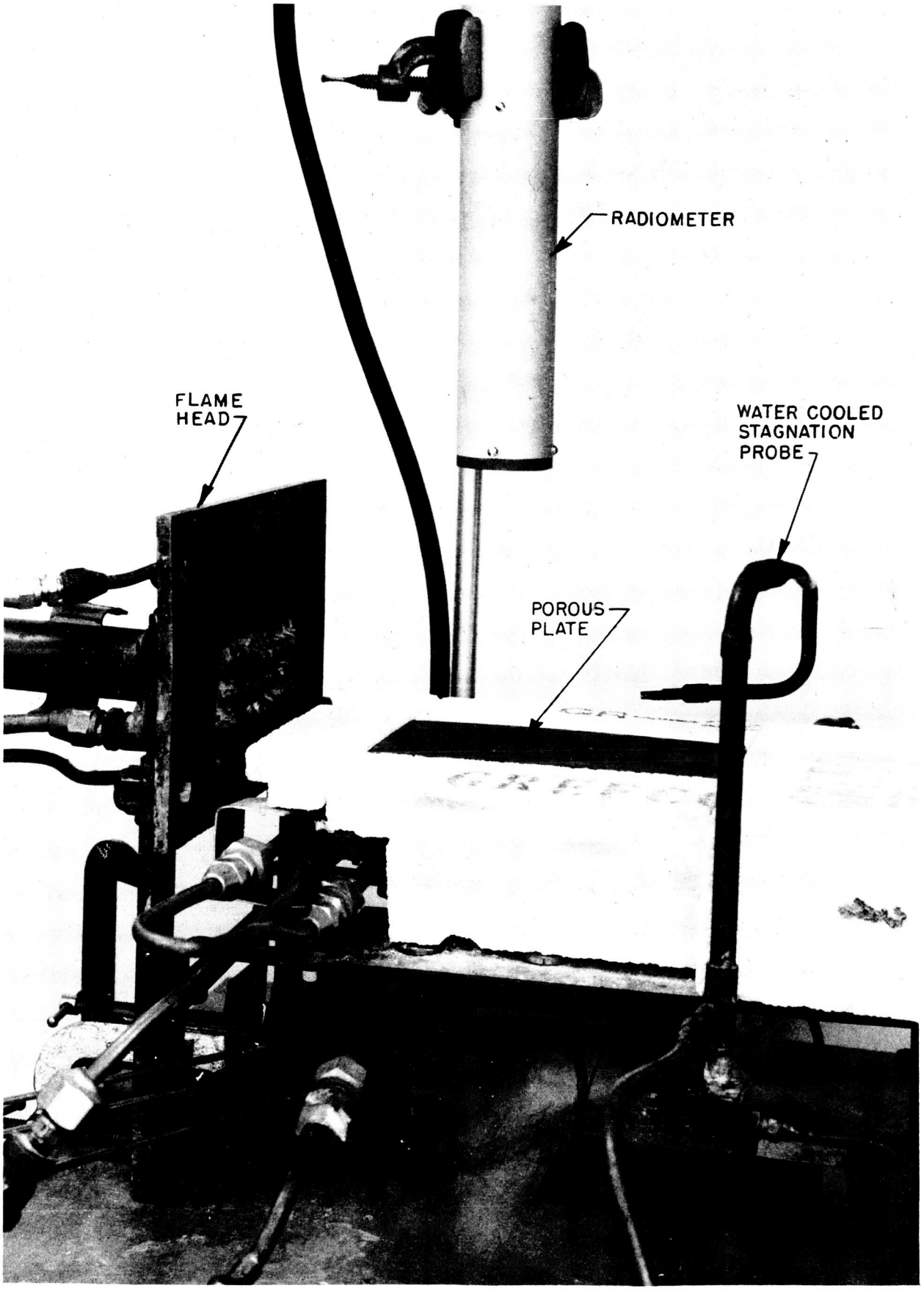

FIG. 2 POROUS SECTION MOUNTED FOR HEATING HYD 8050

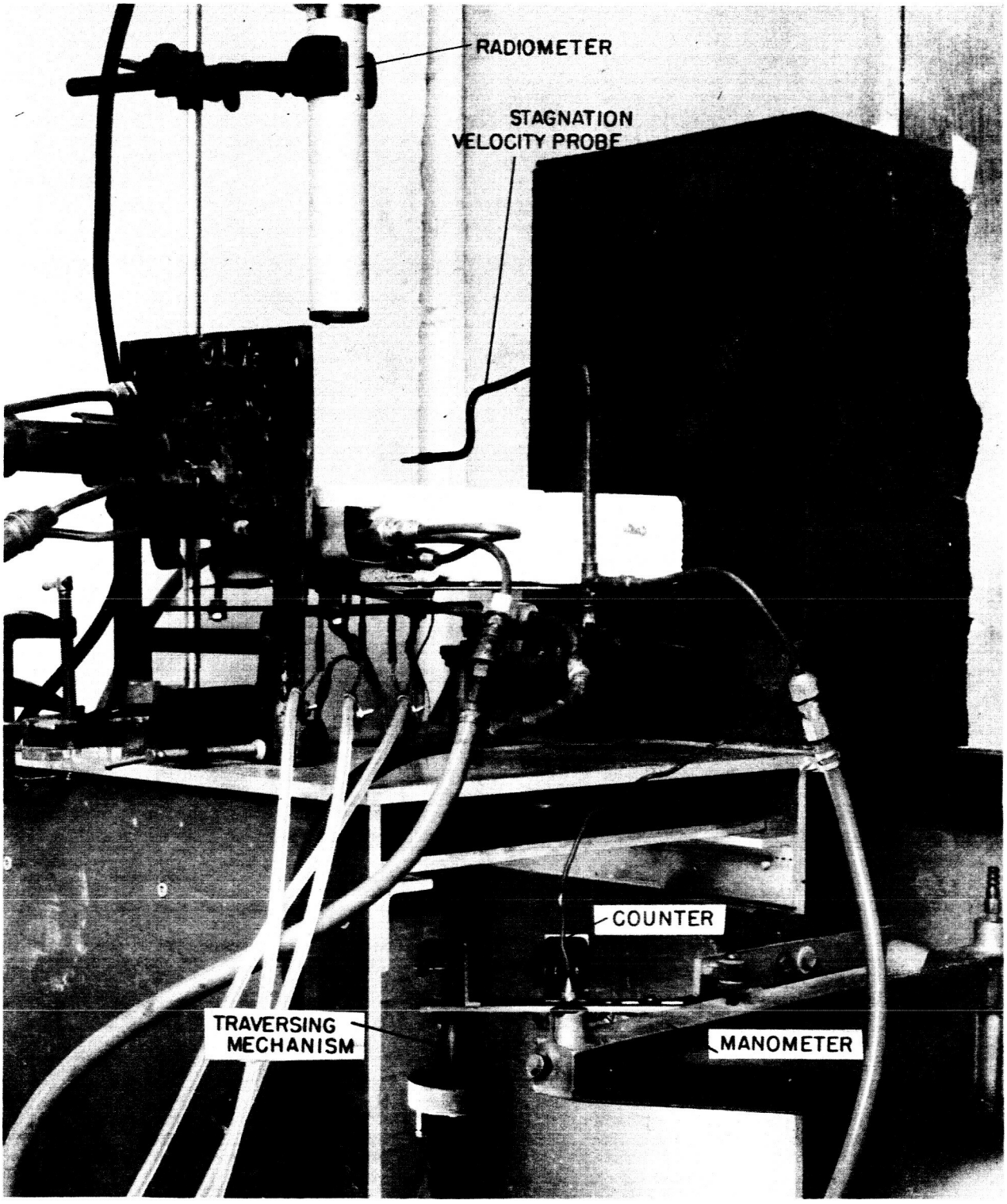

FIG. 3 SYSTEM FOR MEASURING VELOCITY PROFILES

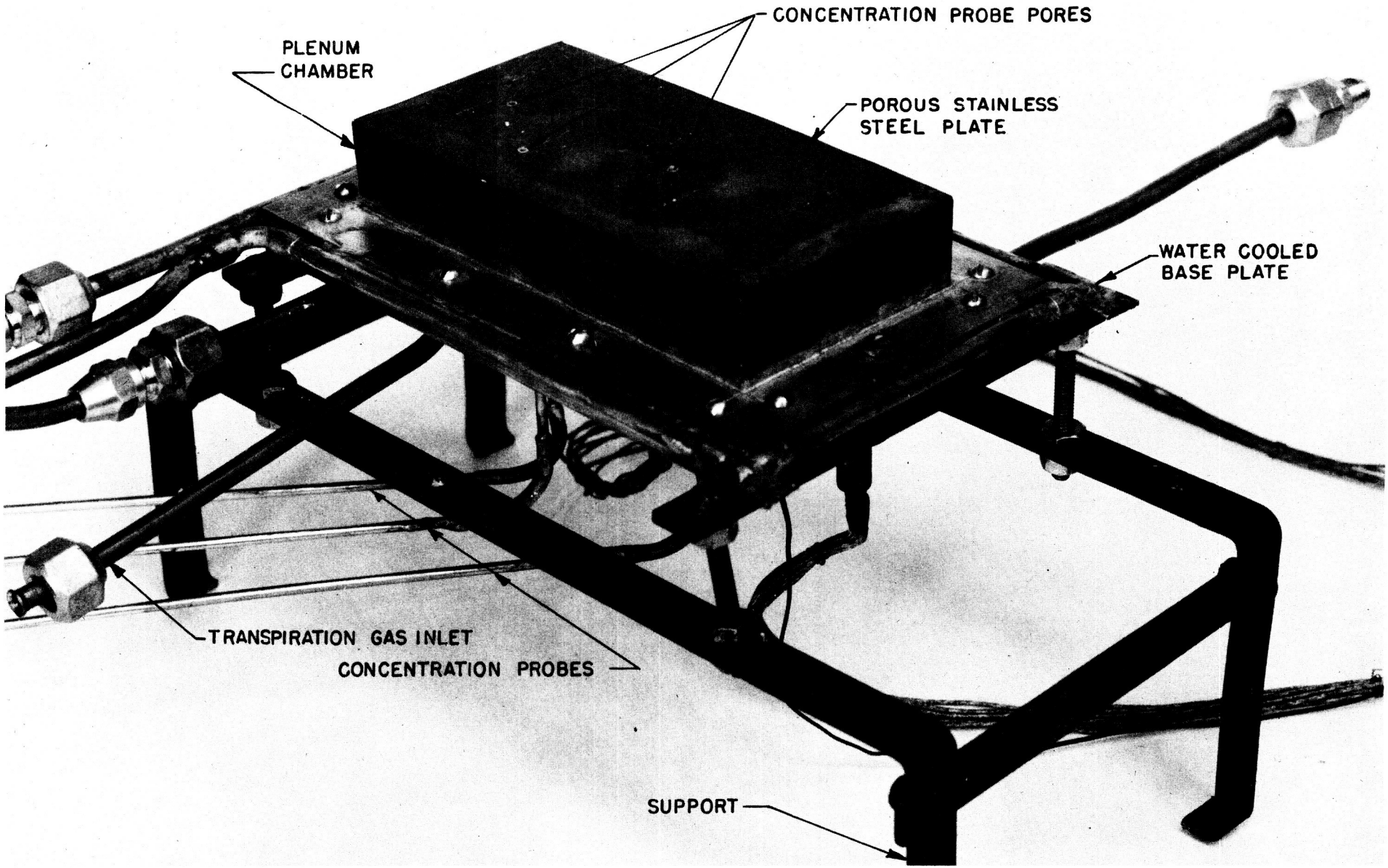

FIG. 4 POROUS TEST SECTION

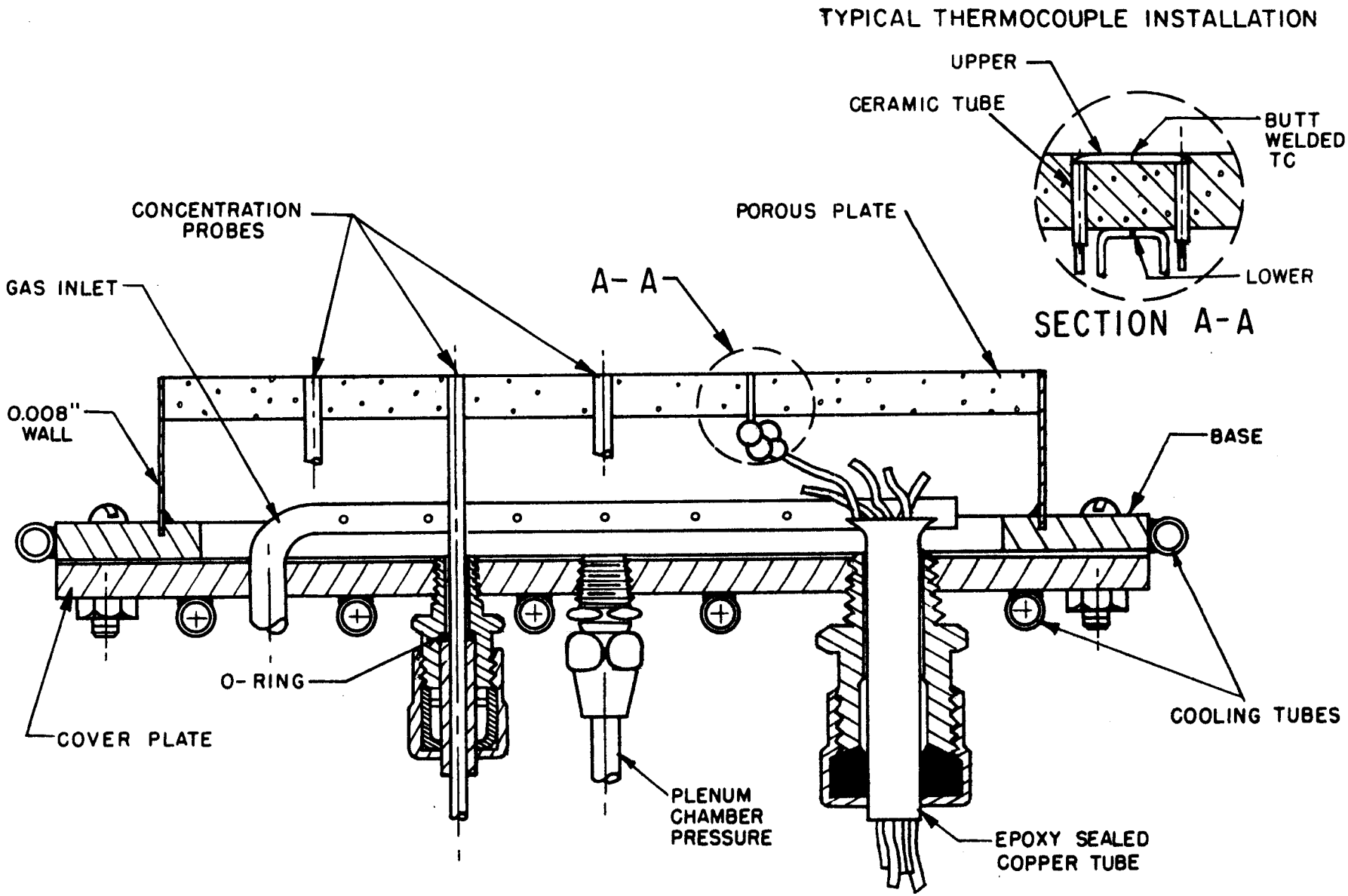

FIG. 5 POROUS PLATE AND INSTRUMENTATION

HUD 8053

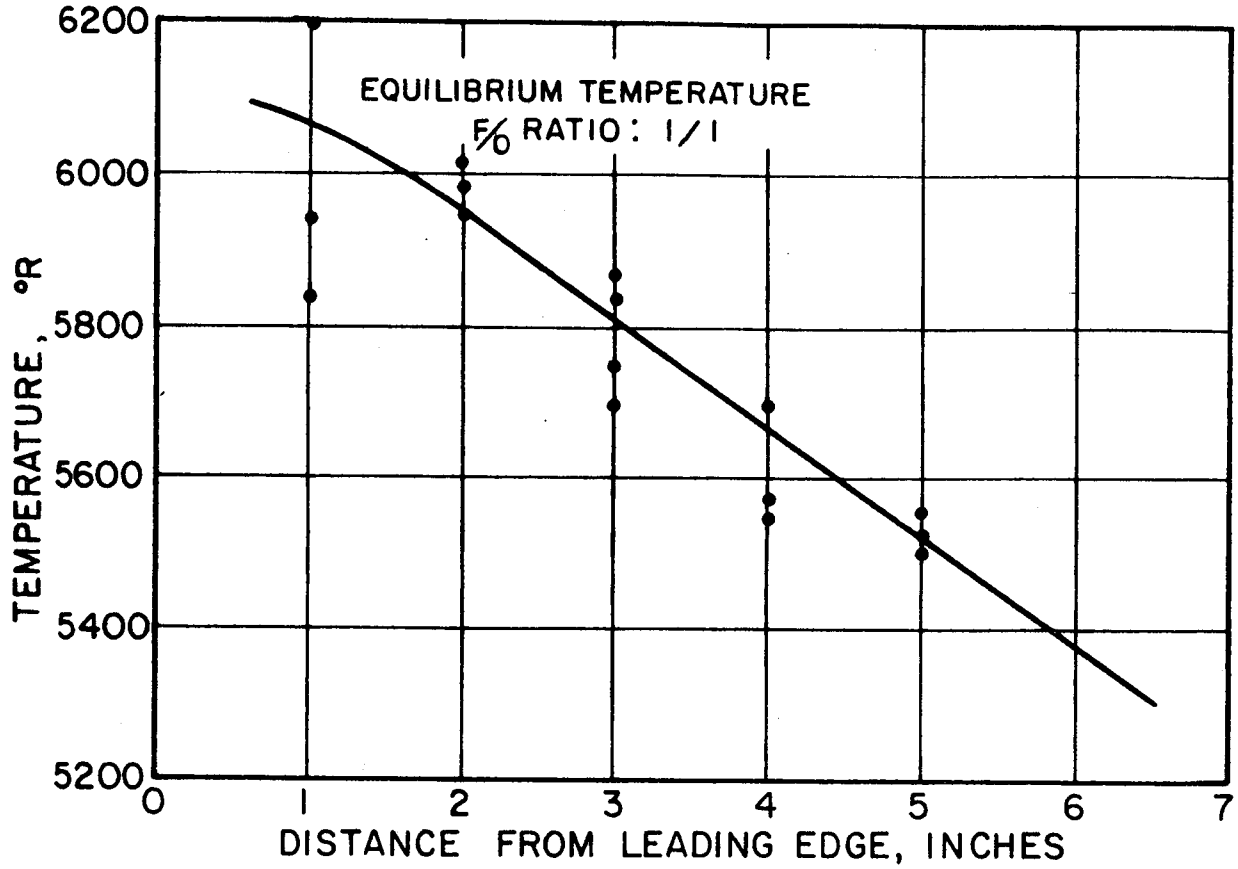

TEMPERATURE DISTRIBUTION ALONG CENTER LINE OF TEST SECTION

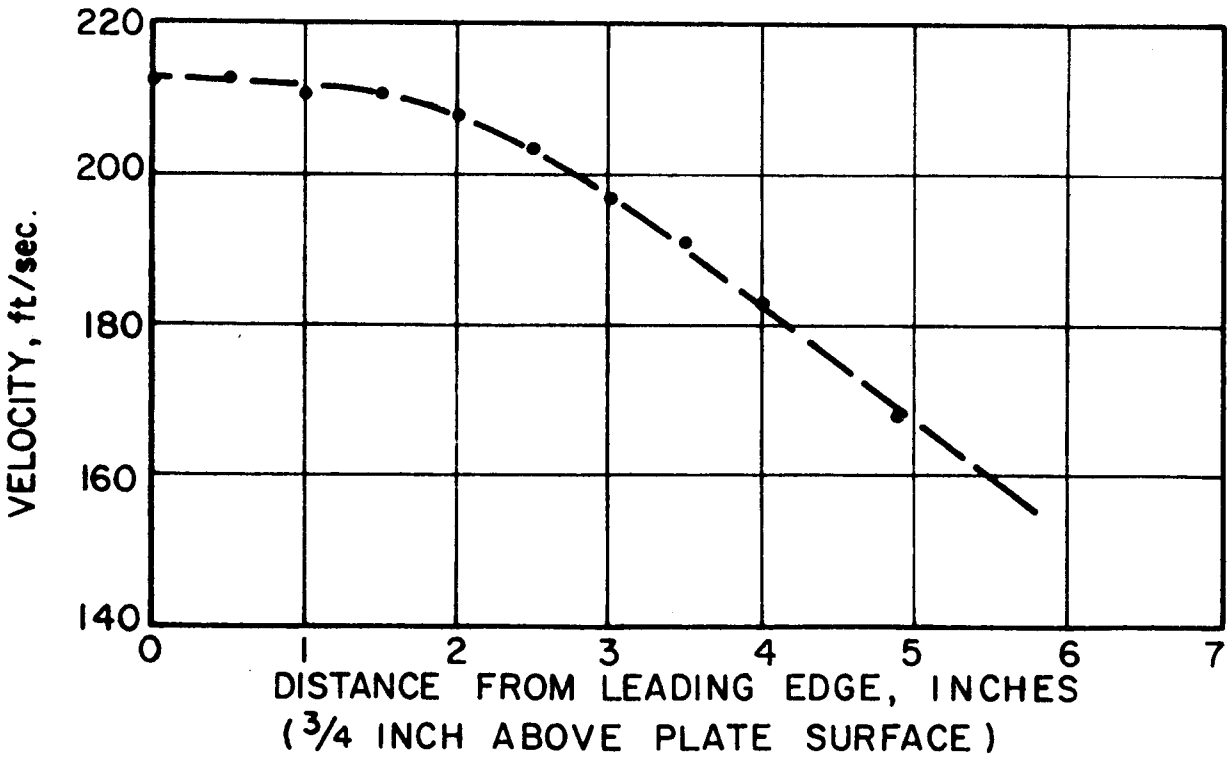

FIG.6 VELOCITY DISTRIBUTION ALONG CENTER LINE OF TEST SECTION

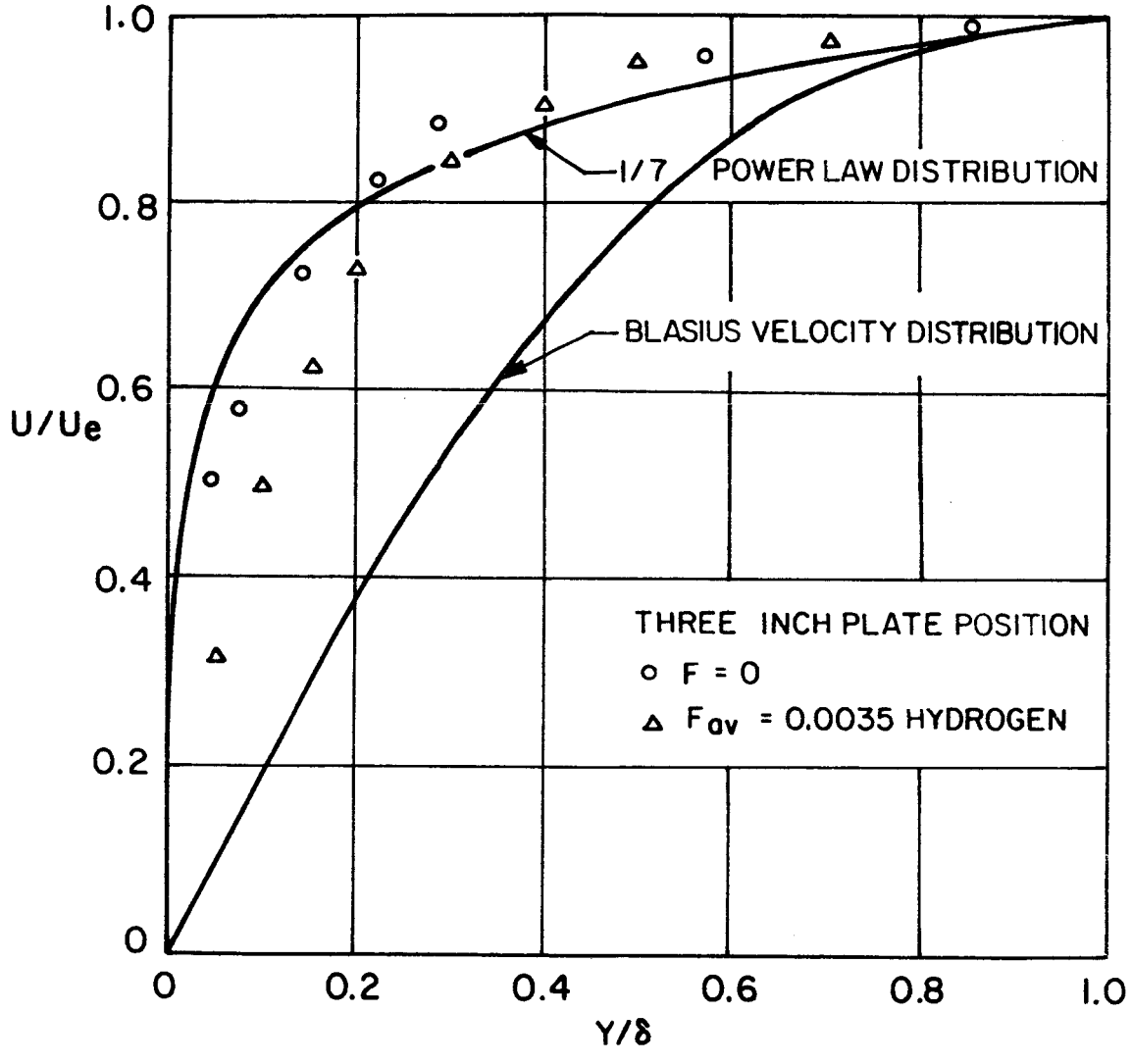

FIG.7 TYPICAL VELOCITY PROFILE

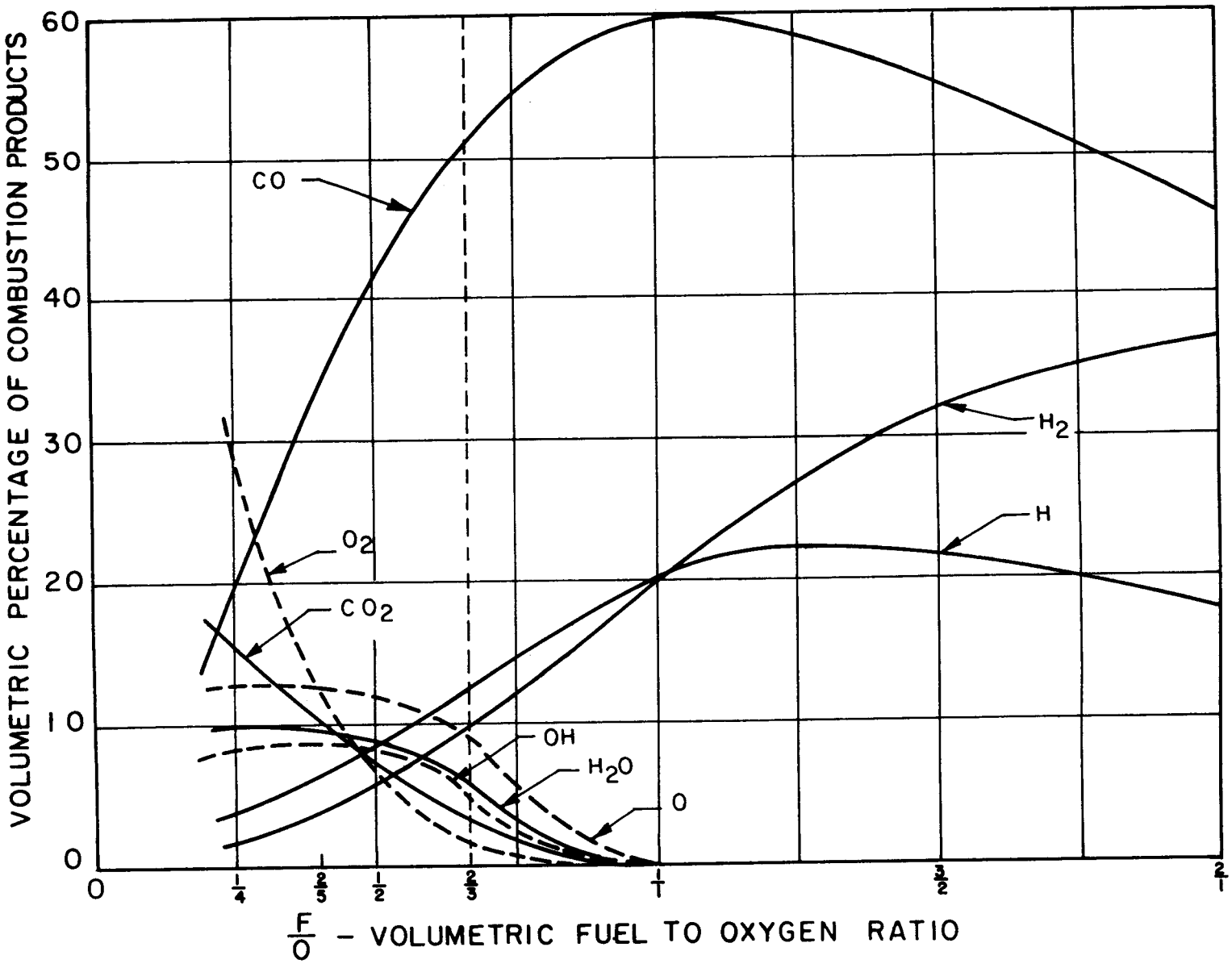

FIG.8 EQUILIBRIUM COMPOSITION OF COMBUSTION PRODUCTS VS FUEL TO OXYGEN RATIO

HYD 8056

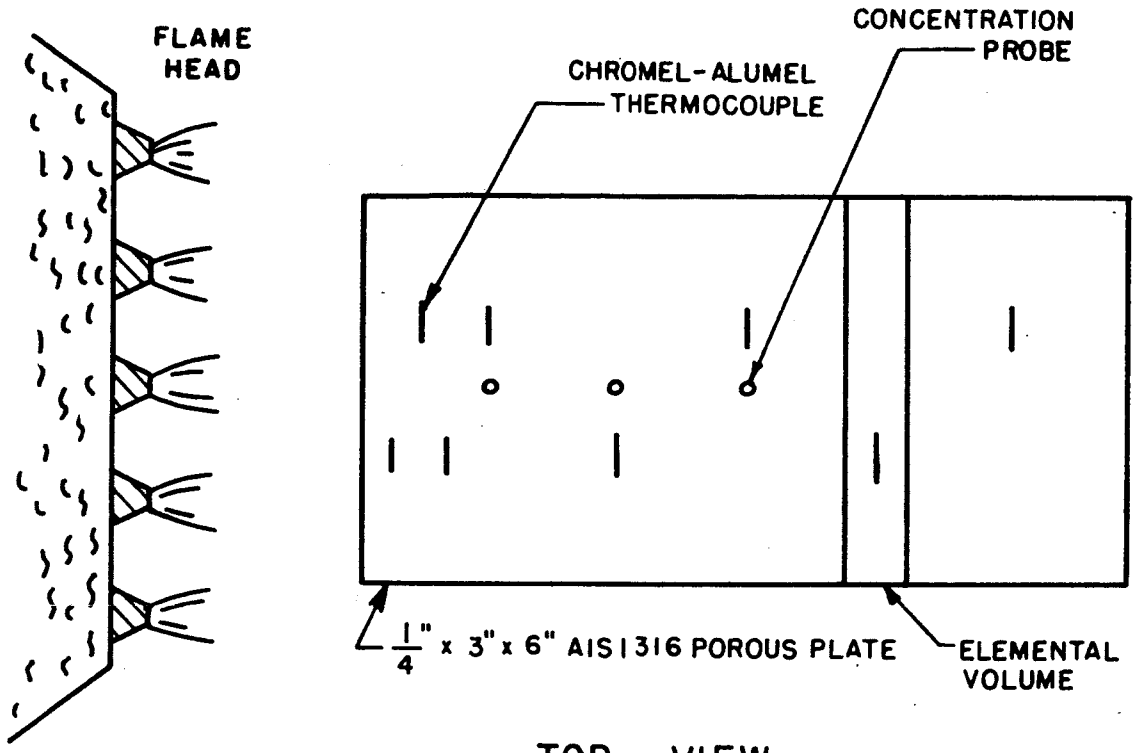

TOP VIEW

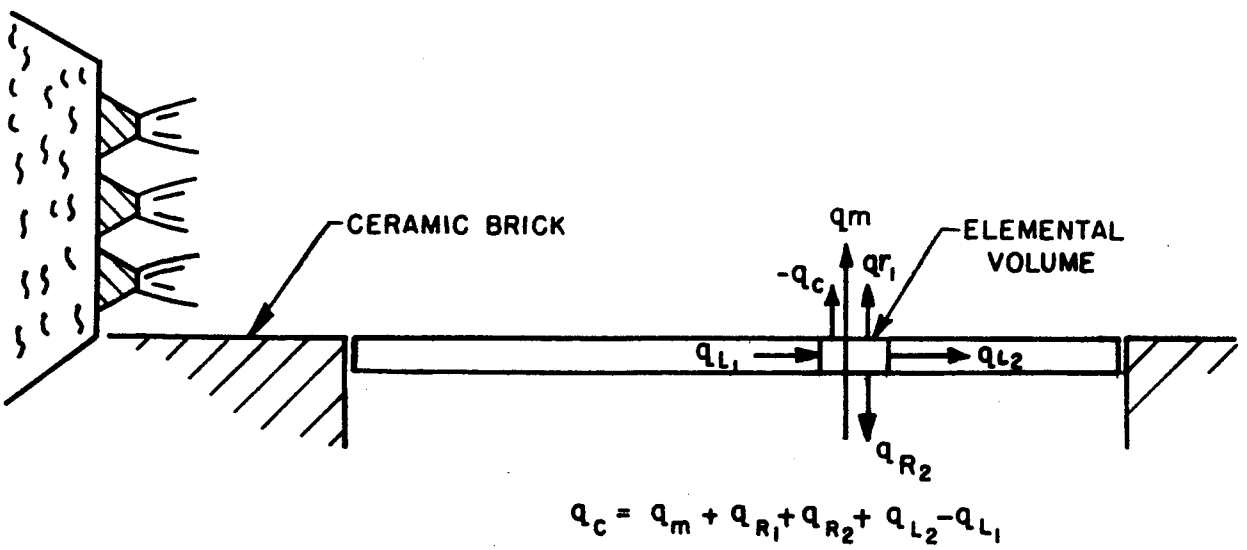

SIDE VIEW

FIG. 9 STEADY STATE HEAT BALANCE

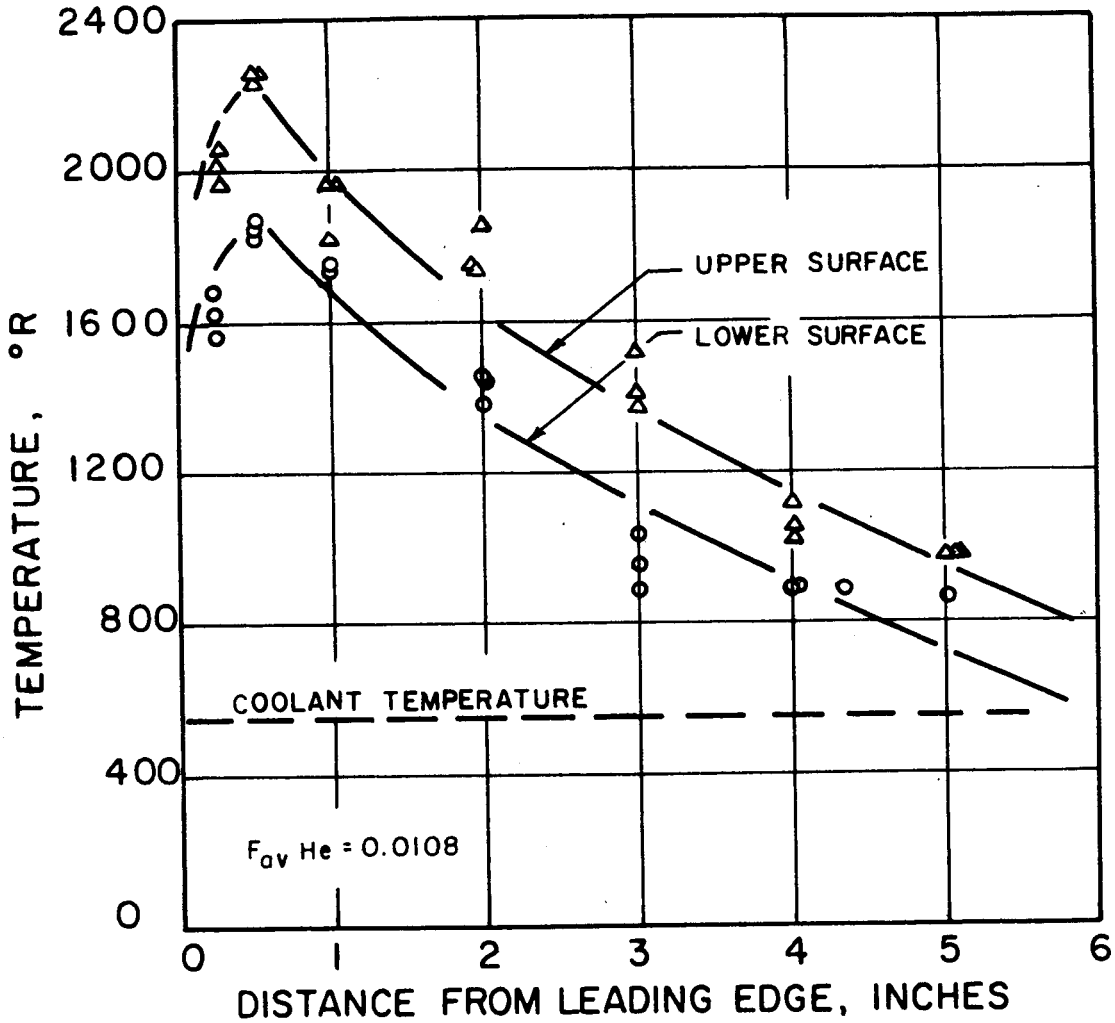

FIG. 10 POROUS PLATE WALL TEMPERATURES

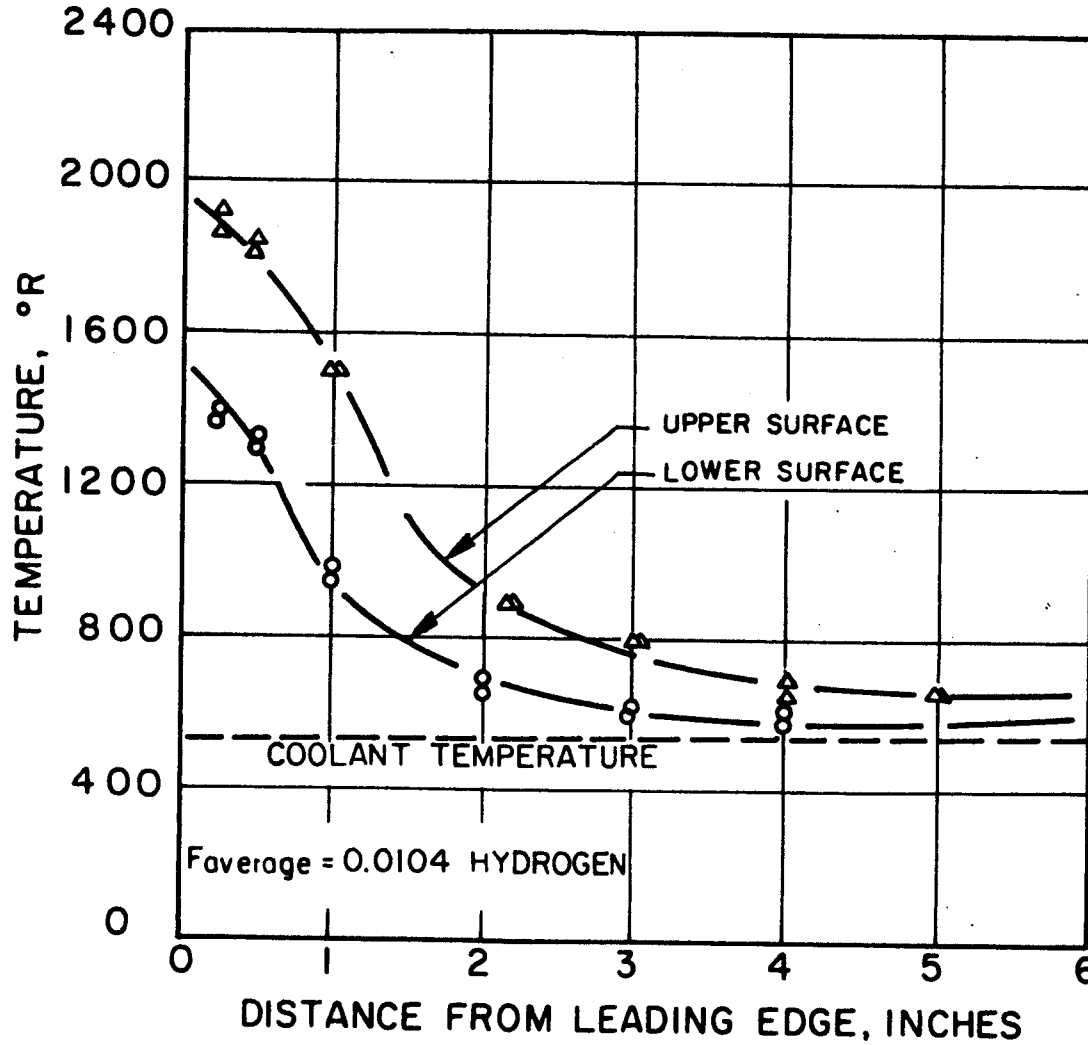

FIG. 11 POROUS PLATE WALL TEMPERATURES

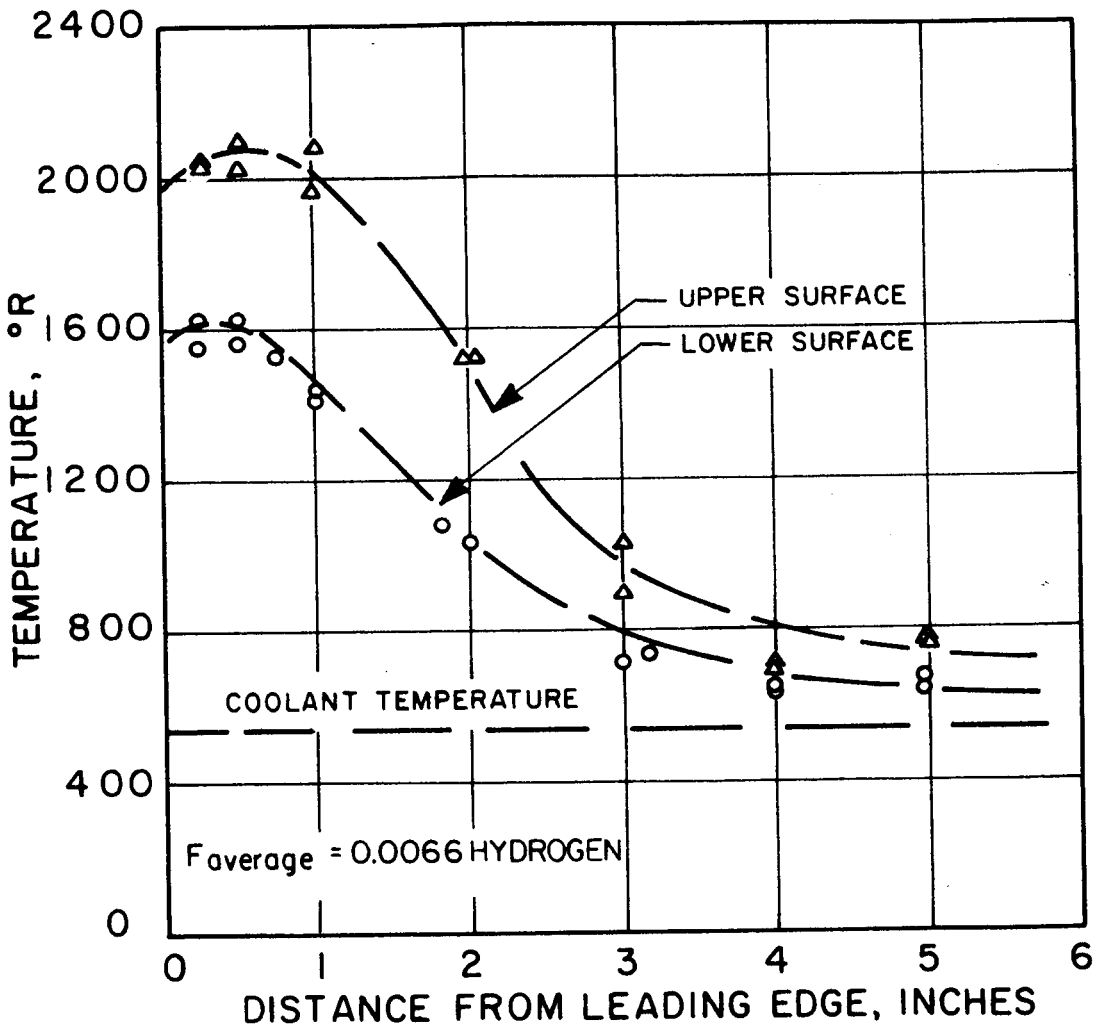

FIG. 12 POROUS PLATE WALL TEMPERATURES

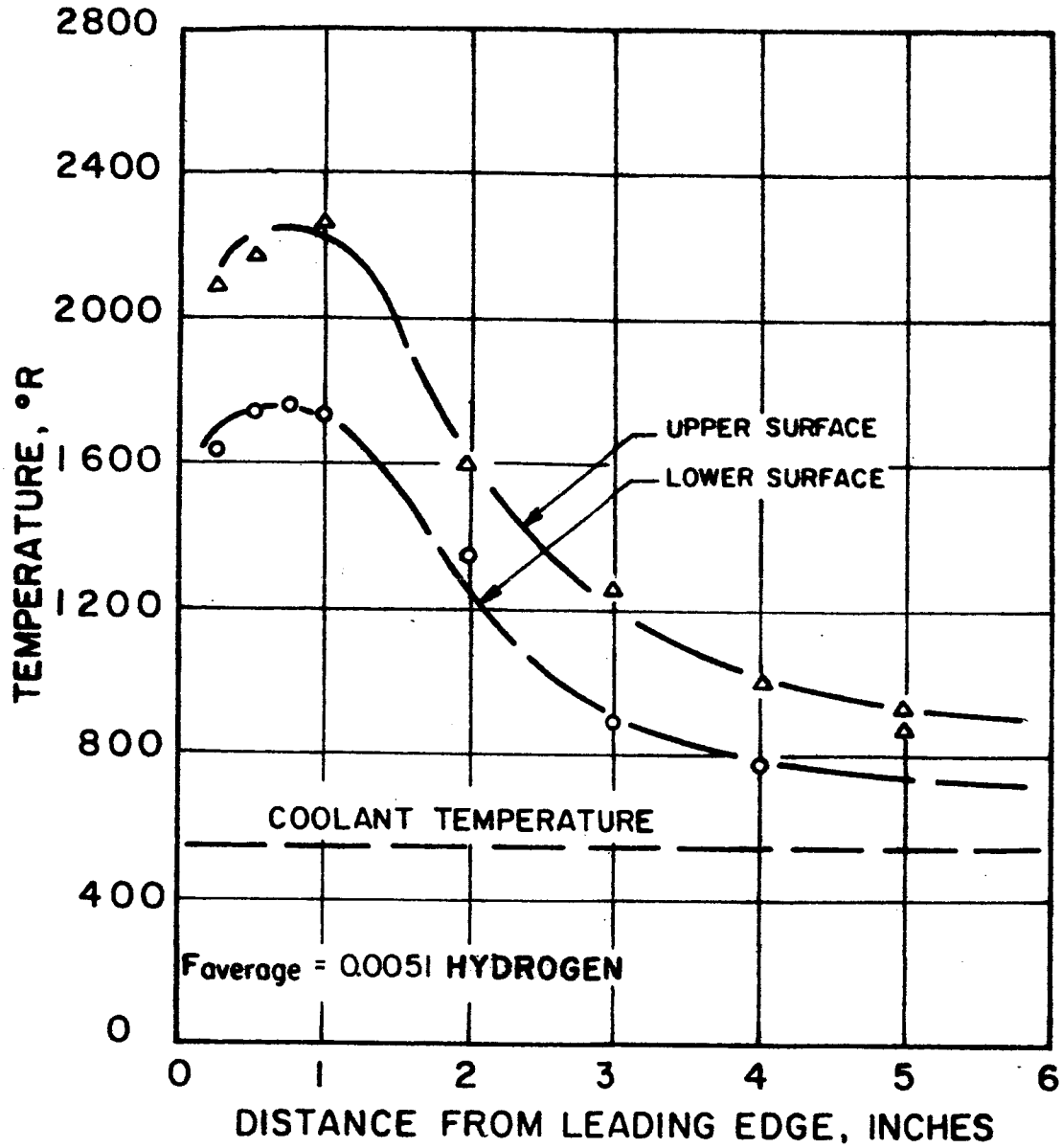

FIG. 13 POROUS PLATE WALL TEMPERATURES

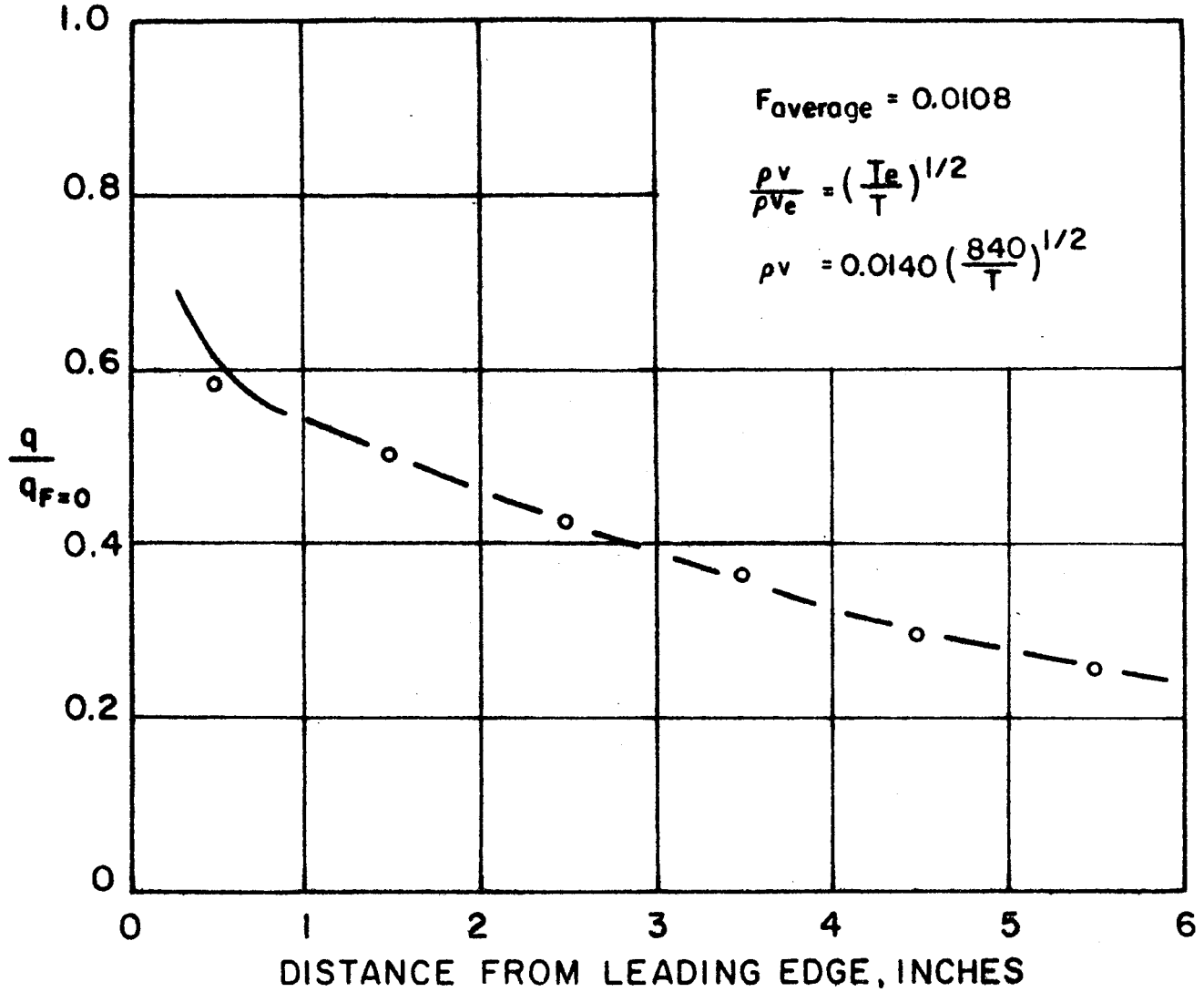

FIG. 14 HEAT TRANSFER RATIO WITH HELIUM INJECTION

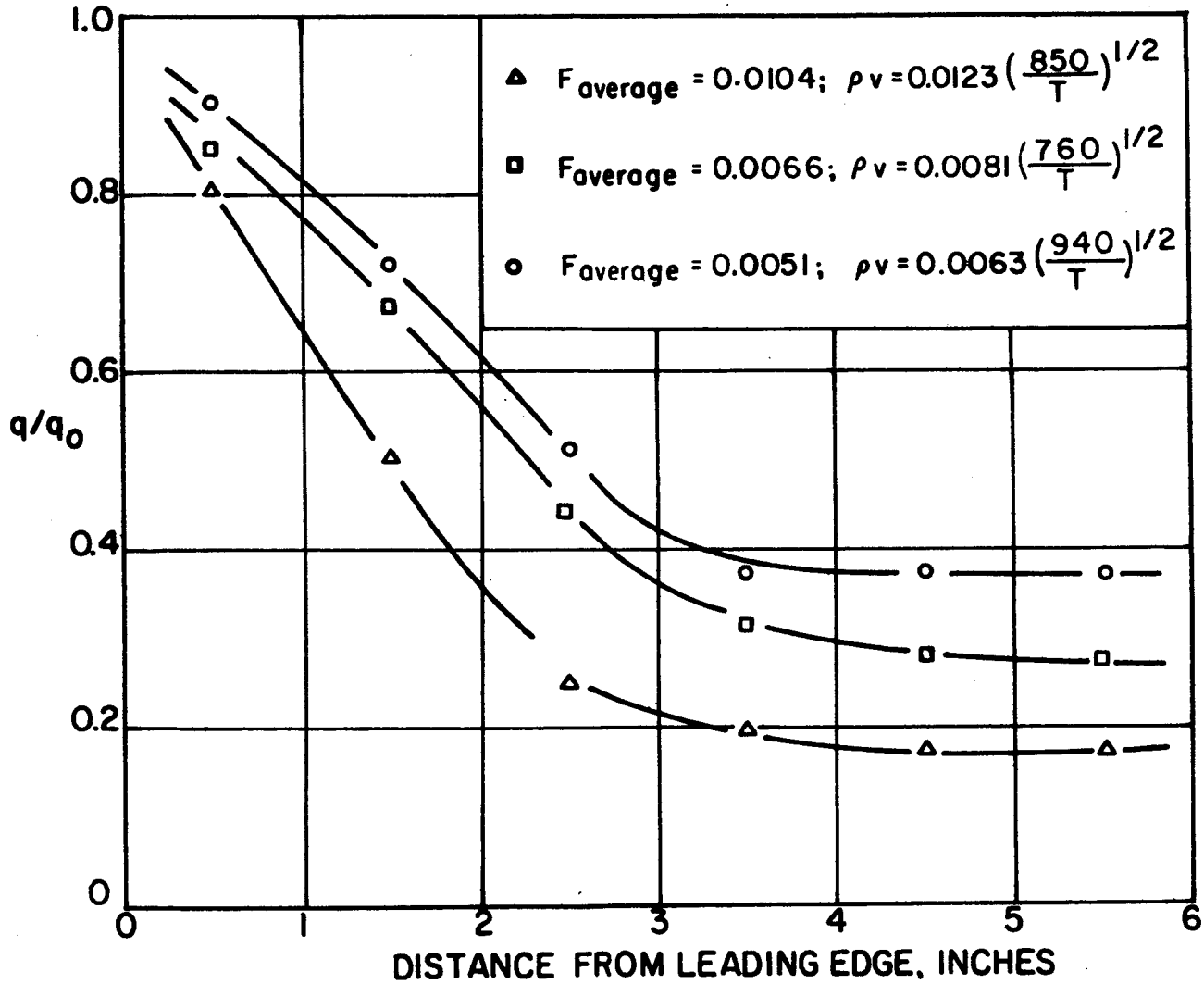

FIG. 15 A HEAT TRANSFER RATIO WITH HYDROGEN INJECTION

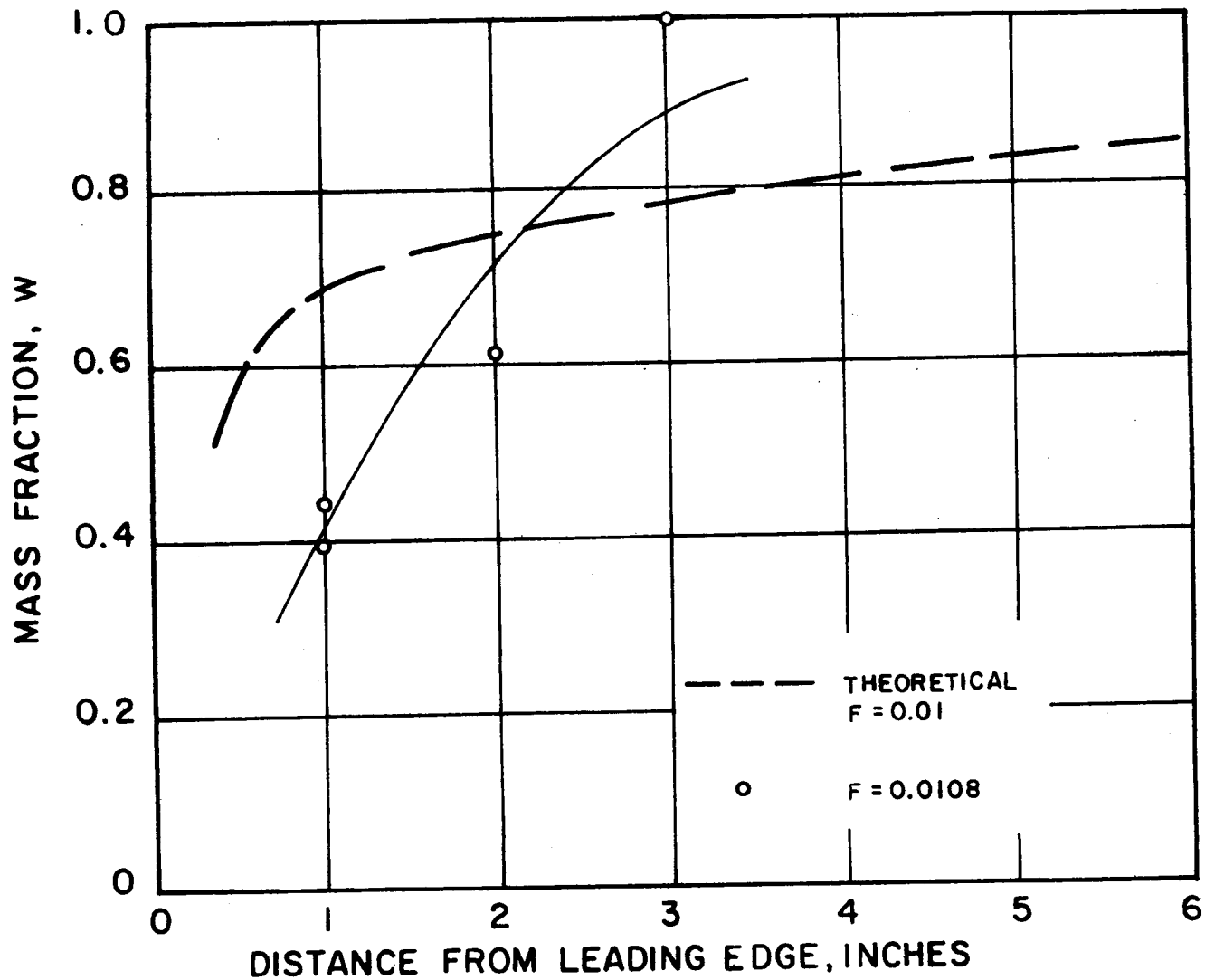

FIG. 16 WALL MASS FRACTION WITH HELIUM INJECTION

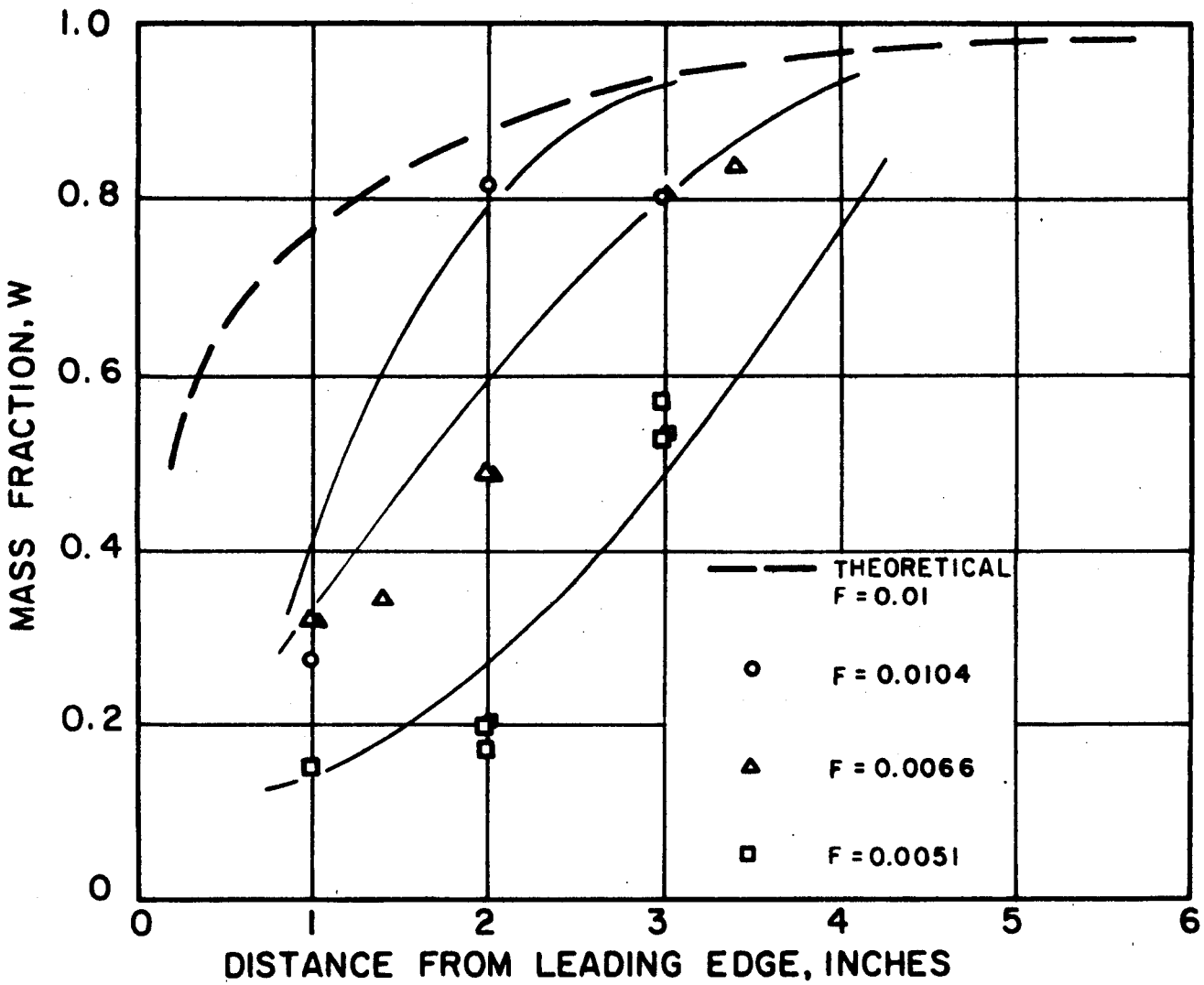

FIG. 17 WALL MASS FRACTION WITH HYDROGEN INJECTION

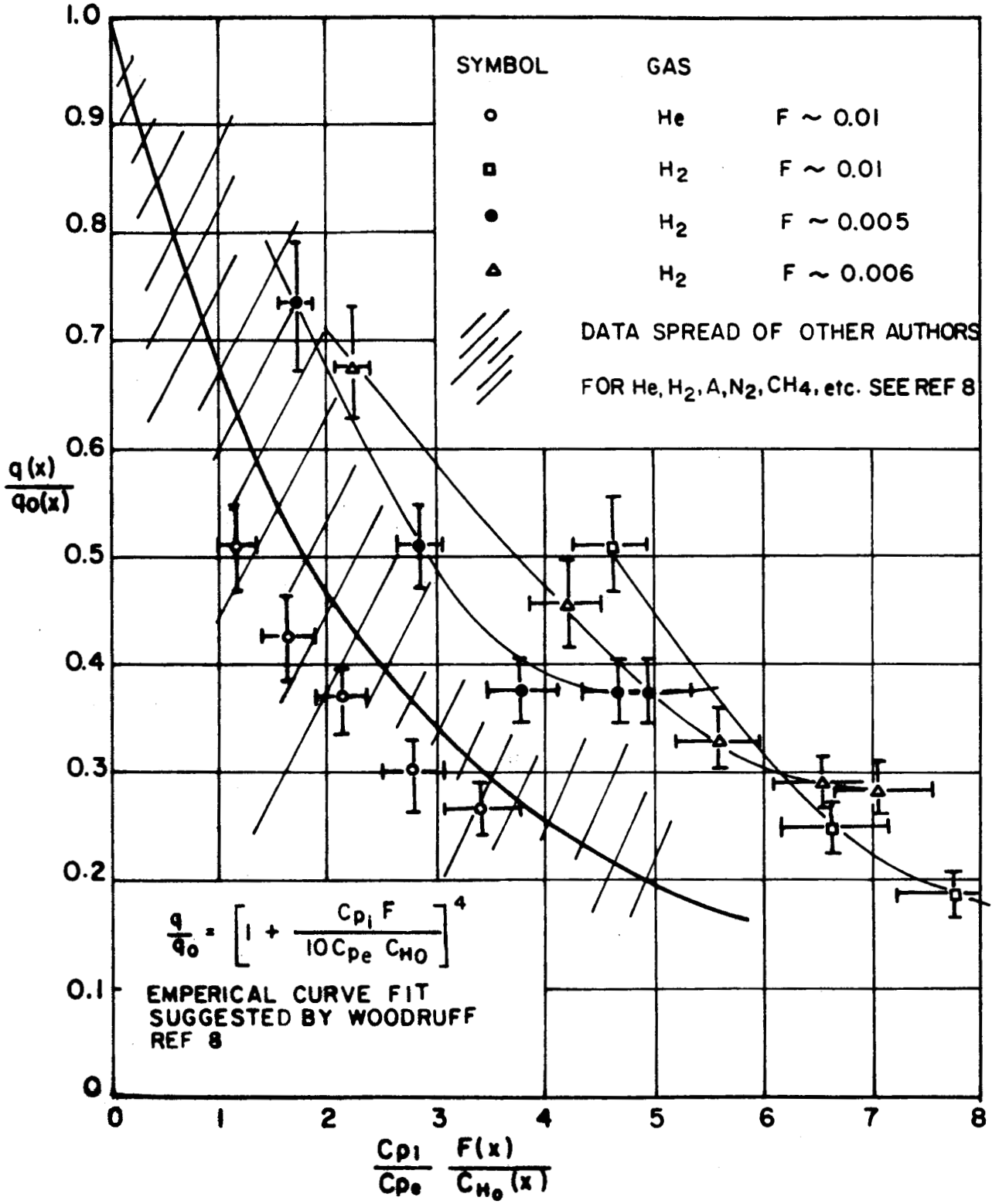

FIG. 18 EFFECT OF FOREIGN GAS INJECTION ON THE TURBULENT, ZERO PRESSURE GRADIENT LOCAL HEAT TRANSFER

APPENDIX A: THERMAL DIFFUSIVITY MEASUREMENTS OF POROUS STAINLESS STEEL

Although extensive information is available for the thermal properties of solid stainless steels, little effort has been made to determine these values for their sintered counterparts, the porous stainless steels. As a result, it was necessary to measure the thermal diffusivity of the AISI 316 porous stainless steel used for the porous wall in this study.

To avoid the problems of steady state measurement (large amounts of time necessary to attain equilibrium before measurements and of the high temperature heat losses) a transient technique for measuring the diffusivity of consolidated materials was used. The apparatus and procedures developed by Boozer[30] were made available through the Petroleum Engineering Department of the University of California, Berkeley. The method used was one in which temperature measurements were made during a period of unsteady state heat flow. Cylindrical samples, 1-1/8 inches in diameter and 2-1/4 inches long, were centered in a electric core furnace. The furnace temperature was controlled to establish a linear rate of temperature rise at the edge of the cylinder. After an initial transient heating period data were provided such that the thermal diffusivity could be calculated continuously over a temperature range from 200 to 1800 °F.

The 2-1/4 inch sample was composed of 9 disks 1-1/8 inches in diameter stacked and drilled as indicated in Fig. A-1. Thermocouple holes were precisely drilled parallel to the axis along isotherms to prevent heat loss and provide accurate measurements. Five 0.070 inch diameter holes were drilled to accommodate Pt-Pt 10% Rh thermocouples within ceramic insulating tubes. The center and three edge Pt-Pt 10% Rh

thermocouples were used to measure the edge temperatures. Two 2-1/4 inch long cylindrical sections of a material whose thermal diffusivity was in the same range as the porous stainless steel were used at either end of the test sample to reduce end effects.

The test sample and end pieces were placed in the two inch diameter firebrick insulated electric core furnace, as indicated in Fig. A-2. The power to the furnace was supplied by a motor driven auto transformer. The furnace was controlled to a linear temperature increase of 22 °F per minute by a Leeds and Northrup Speedomax Type G Controller. The control thermocouple was located close to the inner furnace wall. A schematic diagram of the apparatus is provided in Fig. A-3.

The basic governing equation for the cylindrical flow of heat through a homogeneous, isotropic medium, whose thermal conductivity is independent of temperature, is

$$\frac{\partial^2 T}{\partial r^2} + \frac{1}{r}\frac{\partial T}{\partial r} = \frac{1}{\alpha}\frac{\partial T}{\partial \theta} \qquad \text{(A-1)}$$

Initial and boundary conditions are:

$$\text{I.C.} \quad T(r,o) = T_o \qquad \text{for} \quad \theta = 0 \quad 0 \leq r \leq a$$

$$\text{B. C.} \quad T(a,\theta) = T_o + h\theta \qquad \text{for} \quad \theta > 0 \qquad \text{(A-2)}$$

$$T(o,\theta) \quad \text{is finite}$$

The solution of this set of equations is:

$$T = T_o + h\left(\theta - \frac{a^2 - r^2}{4\alpha}\right) + \frac{2h}{\alpha}\sum_{n=1}^{\infty} e^{-\alpha B_n^2 \theta}\,\frac{[J_o(r,B_n)]}{[B_n^3 J_1(a\,B_n)]} \qquad \text{(A-3)}$$

where B_n = n^{th} root of Bessels equation $J_o(aB_n) = 0$

h = heating rate

a = distance between edge and center thermocouples.

Considering only the linear part of the heating time one may solve for the diffusivity.

$$\alpha = \frac{a^2 h}{4\Delta T} \qquad \text{(A-4)}$$

where α = thermal diffusivity

a = sample radius to measuring points

h = heating rate

ΔT = edge-center temperature differential

Of course for most natural materials, the thermal conductivity is temperature dependent, decreasing with increasing temperature. To evaluate the error in using Eq. (A-4) for a truly variable diffusivity case Boozer[30] solved for temperature distributions in materials for which published temperature-diffusivity data were available and solved for diffusivity using Eq. (A-4). The largest error noted was 25% at the extreme temperature condition. The agreement seems adequate for engineering purposes. Analysis of experimental errors predicted to be included in the measured value of thermal diffusivity was computed to be approximately plus or minus 10%. Several runs over the entire temperature range were made to determine if any accumulative precipitation of carbon or crystal transformations occurred; none were indicated by the data.

The information resulting from the above examination of the porous stainless steel used is summarized in Fig. A-4. It is compared with published values for equivalent solid stainless steel.

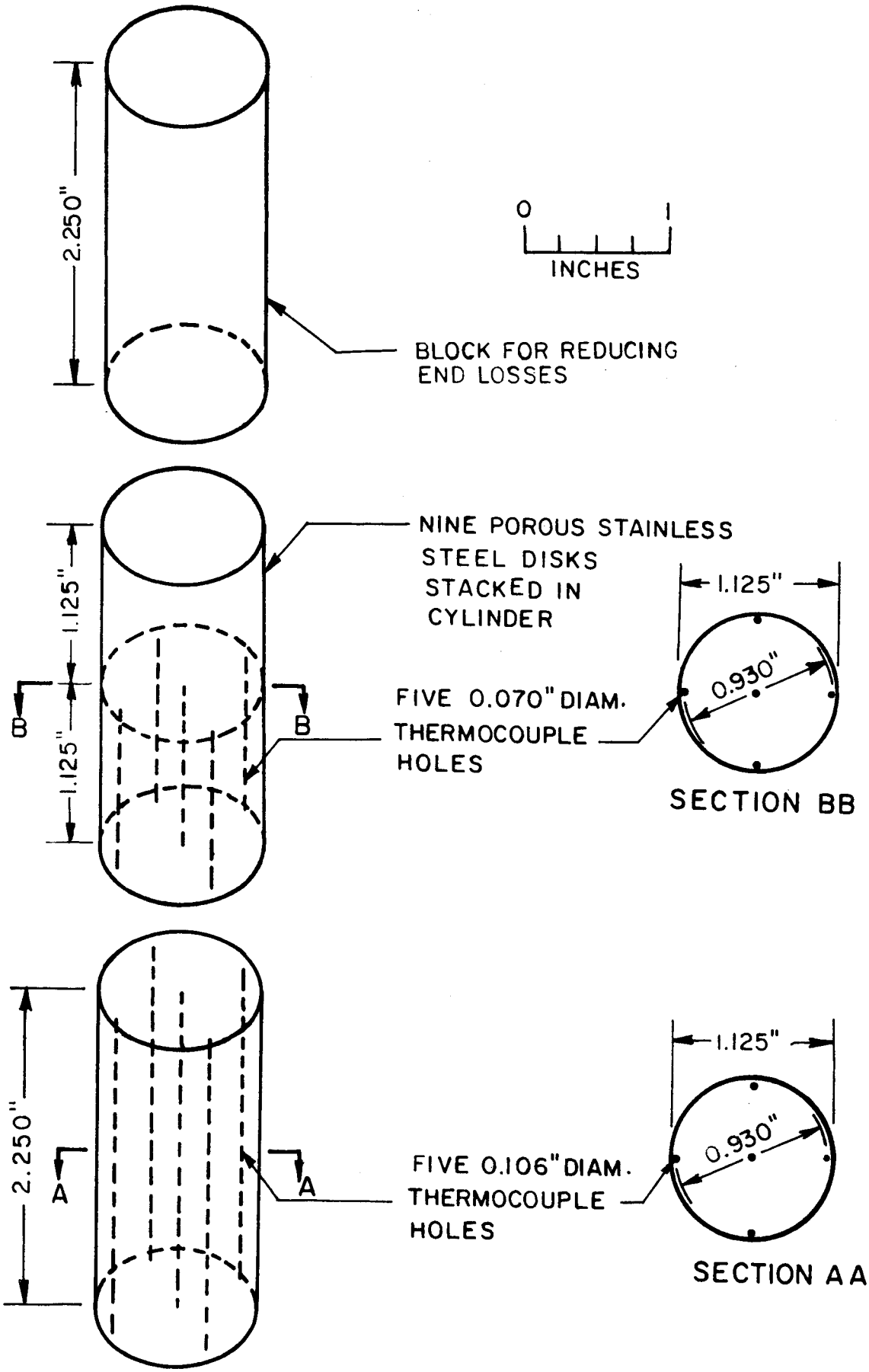

FIG. A-1 TEST SAMPLE SHOWING LOCATION OF THERMOCOUPLE

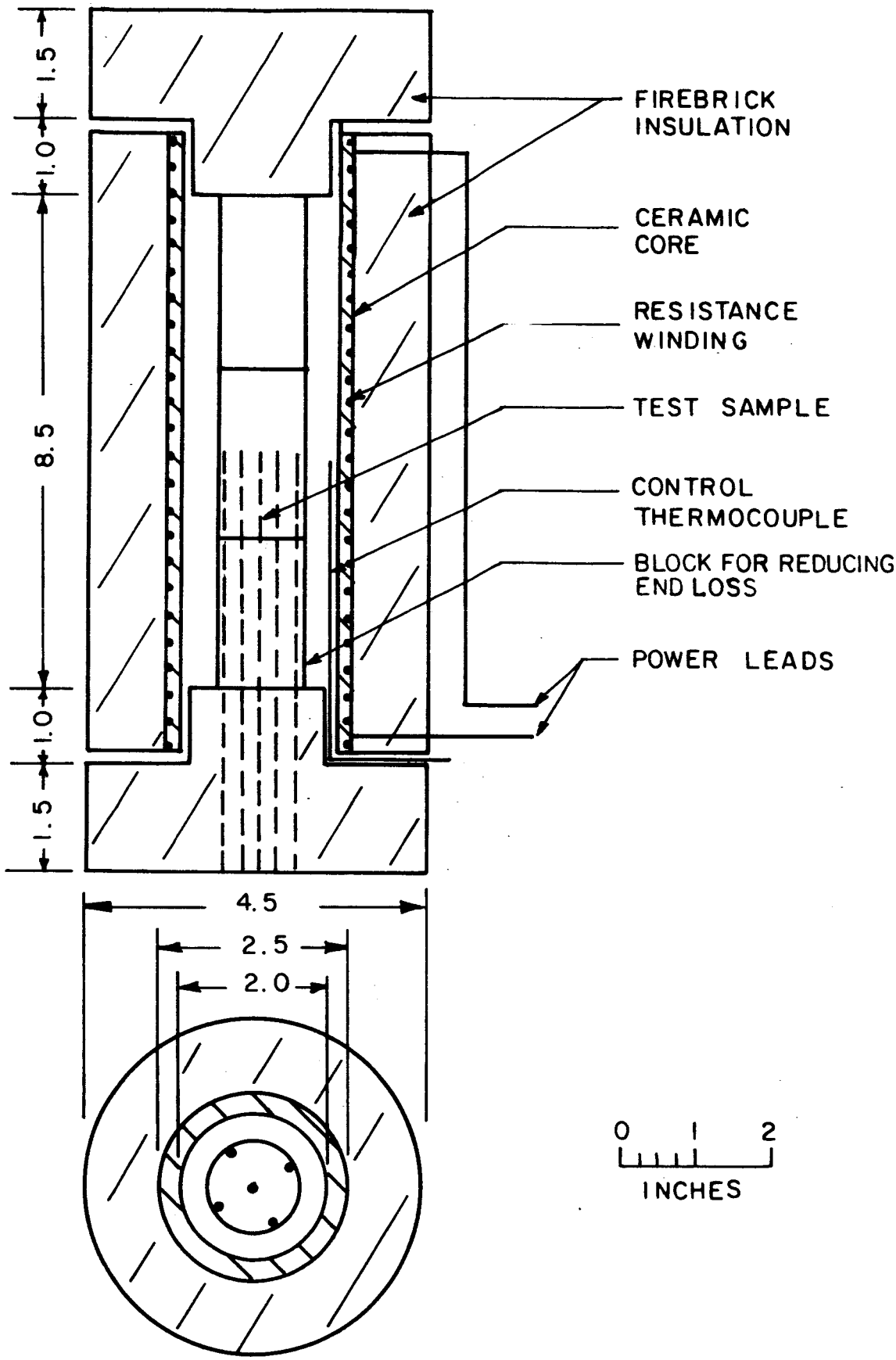

FIG. A-2 DETAILS OF THERMAL DIFFUSIVITY FURNACE

HYD 8068

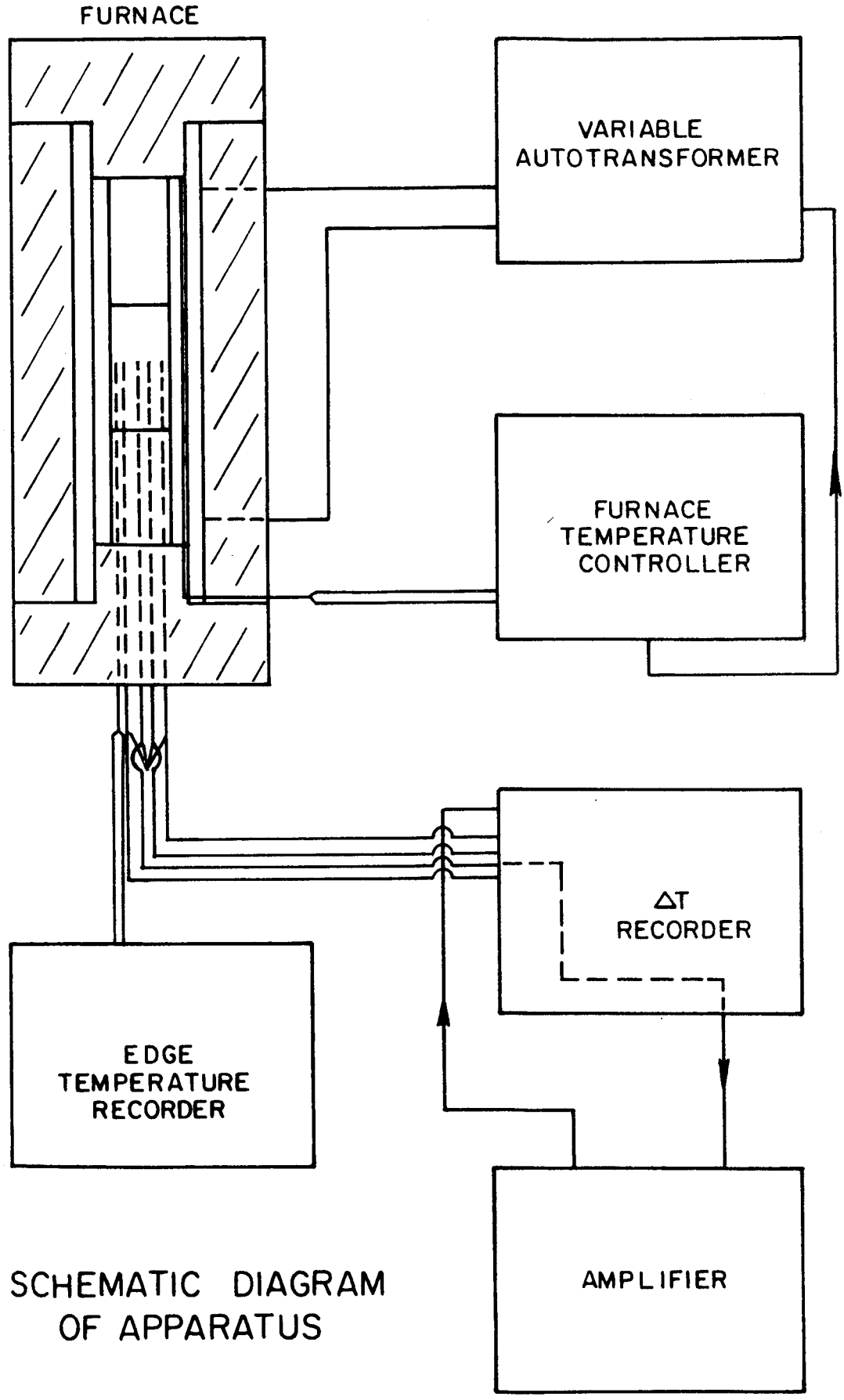

FIG. A-3 SCHEMATIC DIAGRAM OF THERMAL DIFFUSIVITY APPARATUS

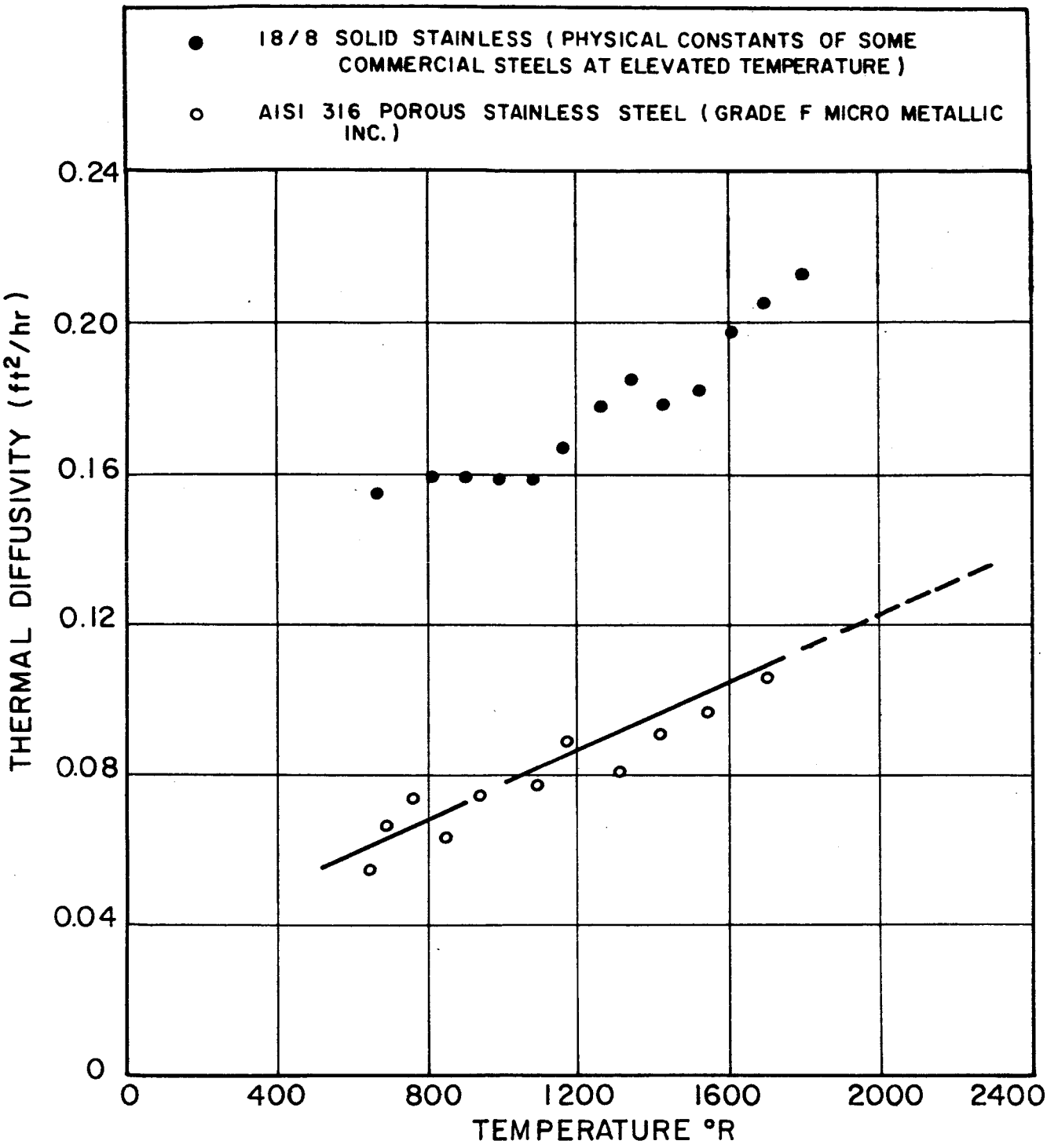

FIG. A-4 THERMAL DIFFUSIVITY OF POROUS STAINLESS STEEL

APPENDIX B: DETERMINATION OF WALL CONCENTRATIONS

In a process where both mass injection of a foreign gas and thermal dissociation of that gas occur, the diffusion of various species due to concentration gradients may govern the magnitudes of both momentum and energy transfer. Although it is desirable to know the local concentration variations across the entire wall boundary layer, it is often sufficient to stipulate concentrations at key points such as at the wall and the free stream in a boundary layer problem. While semi-empirical calculations predict the probable concentration distribution and wall concentration from the free stream concentration and the blowing parameter, the very nature of the approximate nature of this effort makes it desirable to check experimentally such values for at least a few points on the blowing surface.

Due to these considerations small samples of combustion and injection gas were drawn from the porous blowing surface during the various experimental tests and capsuled at atmospheric pressure. These samples were subsequently introduced into a gas chromatograph analysis unit specifically designed for the products present during oxy-acetylene torch operation. The species expected in an oxy-acetylene flame burning neutrally, or in a one to one fuel ratio, are CO, H_2, and H. Under ideal conditions solid C, unburned acetylene C_2H_2, O_2, or any other species are absent. The apparatus was designed to differentiate CO_2, CO, H_2, and N_2. Atomic hydrogen was not expected at the wall, which remained at temperatures below the level of dissociation.

The samples were drawn from the wall surface through small diameter stainless steel hypodermic tubing into sample holders by a low-suction aspirator. A simple aspirator of low-suction type was used in

order that the boundary layer be disturbed the minimum amount and in order that samples obtained be at, or very near, atmospheric pressure. Previous investigators of the gas products in rocket fumes, torches, or plasmas have experienced contamination of samples by the atmosphere whenever the samples were taken or stored at less than atmospheric pressure.

Chromatography is a technique for the separation of components from a mixture or a solution. However, as technically used for quantitative or qualitative study of gas mixtures, the procedure must include not only separation, but also detection of the separated constituents.[34,35]

The separation system normally consists of a two-phase system. One phase is fixed or stationary, and the other is mobile. The stationary phase which tends to absorb and disperse the various constituents of the moving sample phase may be a liquid distributed on a solid support or merely an absorbent solid such as activated charcoal, silica gels, molecular sieves, etc. Elution analysis is usually the preferred method to introduce a sample gas to a chromatograph column of the stationary phase. By this method, the sample mixture is introduced into a continuous stream of carrier gas which moves the individual components through the column at different speeds. Each component will move at a rate depending on its particular affinity for the column material.

Many different types of detectors have been proposed and used in gas chromatography. Among others, these include infrared analyzer, hydrogen flame detector, mass spectrometer, flame ionization, and thermal conductivity cells. The thermal conductivity cell is the most widely used detector. Basically it consists of a hot wire filament held in the center of a small tube or metal block through which the gas passes. The filament is heated with electric current and the temperature rises to some constant

value which depends on the current, nature of the gas, and flow rate. The cells are usually constructed so that they have two sides, a reference side and a sensing side. One or more filaments is placed in each side and made the arms of a Wheatstone bridge. If the two sides of the cell are filled with the same gas and have identical conditions of current and resistance the bridge will be balanced and no signal will be registered. If the thermal conductivity of the gas on the sensing side is lower or higher than the thermal conductivity of the gas on the reference side, then the temperature of the filament on the sensing side will differ from that on the other side and thus this difference may be recorded versus time on a mv recorder.

The apparatus used throughout most of the analysis of samples from the oxy-acetylene flame system was a Beckman GC-2 Gas Chromatograph. It contained a 13X molecular sieve four feet long suitable to separate He, H_2, CO, CH_4, N_2 and O_2, and had a thermal conductivity cell detector. (See Fig. B-1). In order to detect He in a given sample and also in order to accentuate the presence of H_2, nitrogen was used as a carrier gas.

The detector was calibrated with the nitrogen carrier and individual samples of the gases at a given carrier gas flow rate, a given filament temperature, and a given column temperature. This provided information on the linearity of the equipment response at different attenuation settings and sample sizes and the sensitivity factors for the detector's response to various gases.

When two sample components are compared at equal volumetric amounts, then the relative sensitivity factor may be expressed as

$$K_i = \frac{A_i}{A_R}$$

where K_i = sensitivity factor of component i

A_i = integrated signal on area from detector for sample i

A_R = integrated signal on area from detector for reference sample.

To determine the volumetric percent of sample i in a mixture from the chromatograph output response then write

$$x_{iv} = \frac{A_i/K_i' \times 100}{\sum_i A_i/K_i'}$$

In terms of mass fractions

$$w_i = \frac{M_i x_i}{\sum M_i x_i}$$

where M_i = molecular weight of species i.

A typical chromatograph record is shown in Fig. B-2 and concentration results are displayed in Figs. 16 and 17.

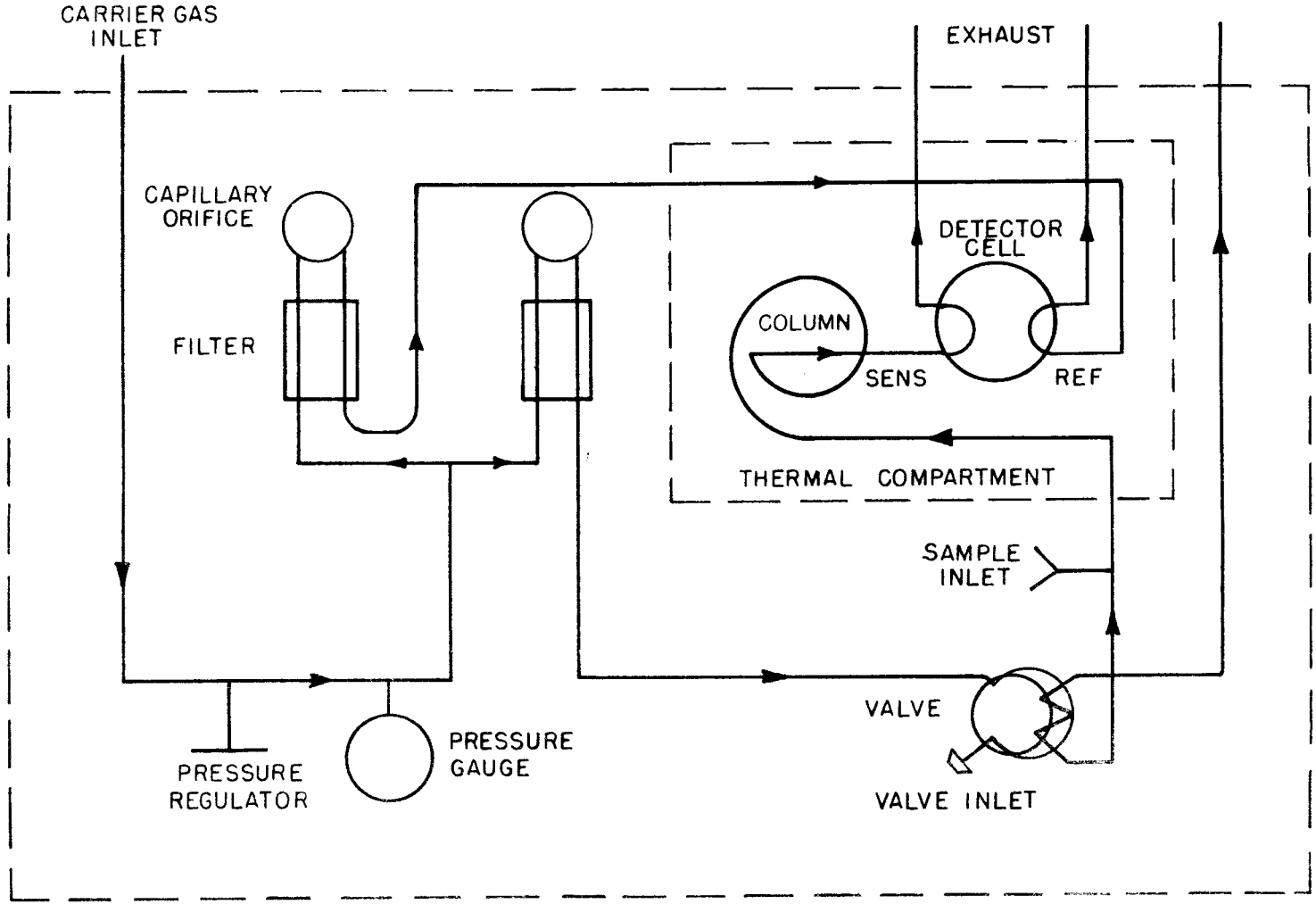

FIG. B-1 FLOW DIAGRAM FOR GAS CHROMATOGRAPH

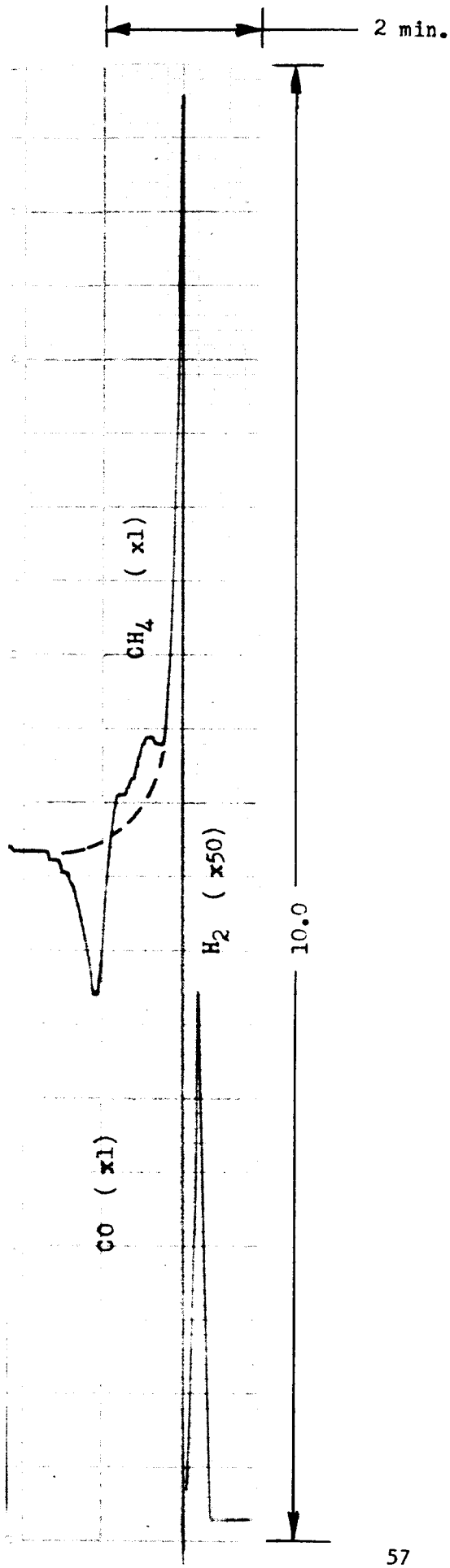

FIGURE B-2: GAS CHROMATOGRAPH RECORD

Beckman GC-2 Chromatograph

Carrier Gas: Nitrogen

Filament Current: 150 ma

Regulator Pressure: 21 psia

Thermal Compartment Temperature: 40° C

Sample: Run No. 37, probe no. 1

Sample Size: 2.5 cc

Sensitivity Factors:

$K_{He} = 3.86$

$K_{H_2} = 7.38$

$K_{CH_4} = 1.00$

$K_{CO} = 0.141$

Corrected Mass Fractions:

$\omega_{H_2} = 10.8\%$

$\omega_{CO} = 89.2\%$

APPENDIX C: ERROR ANALYSIS

The propagation of random errors into the results of an experiment limits the extent to which conclusions may be drawn from empirical data. Hence it is important to fix a value to the "uncertainty" associated with numbers obtained directly or indirectly through experimentation. The results of statistical analysis may be transposed into a scheme to determine the probability that any given point of reduced data is within a certain allowable deviation from the true condition.

By a simple procedure of expanding possible errors and their effects in Taylor series and comparing this with the structure of the standard statistical term, "standard deviation," one may express the probable error in a function $u(x,y,z)$ due to random variation in its independent variables x, y, z as

$$\frac{r_u}{u} = \sqrt{\left(\frac{\partial u}{\partial x}\right)^2 \left(\frac{r_x}{u}\right)^2 + \left(\frac{\partial u}{\partial y}\right)^2 \left(\frac{r_y}{u}\right)^2 + \left(\frac{\partial u}{\partial z}\right)^2 \left(\frac{r_z}{u}\right)^2} \qquad \text{(C-1)}$$

where r_u = probable error (any point of the data has a one to one chance of being within r_u of the actual value u)

r_x, r_y, r_z = probable errors in independent variables determined from instrument least count and experimenter's intuitive estimation of data value.

Several pertinent functions and their probable variations are discussed below.

Free Stream Flame Temperature:

Although Russ predicted a maximum variation of ±150°R in measurements due to variations from person to person, variation in the flame, etc.,

it was felt that improved instrumentation and procedures supported a probable error of ±50°R here.[12]

Free Stream Velocity:

Evaluation of Eq. (3.11) as outlined above will lead to the following relation:

$$\frac{r_u}{u_e} = \sqrt{\frac{1}{4}\left[\left(\frac{\delta\Delta h_e}{\Delta h}\right)^2 + \left(\frac{\Delta T_e}{T_e}\right)^2 + \left(\frac{\delta p_e}{p_e}\right)^2 + \left(\frac{\delta M_e}{M_e}\right)^2\right]} \qquad (C\text{-}2)$$

Accepting a least count for the inclined manometer term Δh of 0.01 inch, this reveals a probable error of 1.4%.

Total Mass Flow Rate Injected Gas:

The controlling parameter turns out to be the scale reading of the gas flowrator. Since this instrument may be easily read within 0.02 SCFM of the average setting of 2 SCFM, the probable error is estimated to be only 1%.

No Transpiration Heat Flux:

Equation (3.14) may also be evaluated in terms of Eq. (C-1). There may be a probable error in the caloric rise in heat of 3%, a radiation error of up to 12.2%, and an error in the estimated heat loss to the brick of 6.5%. These all combine, however, into only a probable error of 4.25% in q_o when the wall temperature is 2000°R. Most significant uncertainties are the estimated plate emissivity and the interpretation of the slopes of recorded temperatures.

Wall Temperature, Plate Properties, and Plate Emissivity:

Although errors were inherent in the wall temperature measurements of the porous plate due to calibration of the Visicorder and breakdown of the thermal properties of the junction during the experiment, it was felt that faired data were valid within ±100°R at 2000°R.

On the basis of Boozer's estimation of the error inherent to his diffusivity measuring technique (Appendix A) the properties of the porous stainless steel were assumed accurate within ±10%.

The porous plate emissivity value of 0.65 was assumed within ±0.10 of its true value. The order of magnitude measured is of that predicted by Eckert for porous materials.

Heat Fluxes with Transpiration:

The heat flux with transpiration was calculated using Eq. (3.8). The sensible energy rise of the injected fluid was felt to be accurate to ±5.65% due to variations in local mass injection or wall temperature. The radiative portion might vary ±15% primarily due to the estimation of the emissivity. Probable error in streamwise wall conduction was ±16.6%. Gaseous radiation might vary 100%.

The net effect on the heat flux term for hydrogen injection at the 1/2 inch plate position would be a probable error of ±7.7%, slightly less for helium injection.